Collected papers dedicated to the 2nd anniversary of establishment of

RESEARCH & DEVELOPMENT CENTRE FOR LOW-COST PLASMA AND NANOTECHNOLOGY SURFACE MODIFICATION – *CEPLANT*

1.12.2010 – 1.12.2012

CEPLANT
Research & development centre for low-cost plasma and nanotechnology surface modifications

EUROPEAN UNION
EUROPEAN REGIONAL DEVELOPMENT FUND
INVESTING IN YOUR FUTURE

2007-13
OP Research and Development for Innovation

s1425

Preface

This volume of Chemical Letters is devoted to current R& D activities of the Regional R&D center for low-cost plasma and nanotechnology surface modifications established as a part of the Institute of Physical Electronics (IPE) at Faculty of Science, Masaryk University in November 2010 in the Operational Programme Research and Development for Innovation. The Centre is a continuation and extension of the more than 50 years lasting tradition of applied plasma physics research at the Department of Physical Electronics, which resulted in several innovations successfully transferred into the industry, the project plan is to launch highly focused applied research of plasma sources and plasma processing development, strategically targeted on industrial end-users.

At IPE the research in applied plasma physics was started more than 50 years ago by prof. Václav Truneček, who was at that time the head of the Institute. His pioneering research of fundamental physics of atmospheric-pressure RF plasma torches launched also fast and systematic developments of the related industrial applications, as well as spectroscopic and microwave diagnostic techniques. Thus already in the early sixties the first research papers were published and the RF plasma torch was successfully tested by company Kavalier Sázava for welding of large diameter glass tubes.

In the mid-sixties the research activities of IPE expanded also to the field of fundamental and applied plasma chemistry. In response to the demands of Czechoslovak industry the team led by prof. Vratislav Kapička and prof. Jan Janča, the former students and successful followers of prof. Truneček, was studying for example the plasma burning and etching, a wide spectrum of methods for plasma depositions including CVD, plasma polymerization, diamond-like thin layers, as well as the deposition of nanocomposite layers and carbon nanostructures. The techniques developed were protected by 12 awarded patents. From the mid-nineties the research activities were extended also to atmospheric-pressure plasma chemistry, first of all to the high-pressure plasma applications for surface activation and cleaning of polymer and metal surfaces, and highly-effective ozone generation. These applications initiated also intense research in the field of high -pressure gas discharge physics aimed at the development of several types of novel atmospheric-pressure plasma sources. The successful research work in the field of atmospheric-pressure plasma chemistry, including several industrial projects, created a base for the establishment of the Center, which covers the major part of the current research activities at INP. The Center is expected to provide practical solutions of technological problems, above all for small and medium-sized enterprises in the Czech Republic. The long-term vision is to create the research team that will be sought after R&D partner also for large international corporations.

The second year of a new institution like the Centre is always likely to be one where consolidation develops alongside innovation and experiment. The short papers collected in this volume present current research lines in the field of applied plasma chemistry at the Centre and collaborating institutions in the Czech Republic.

Prof. Mirko Cernak
director
R&D Center for Low-Cost Plasma and Nanotechnology Surface Modifications
Masaryk University, Brno

IMPORTANCE OF POLYPROPYLENE FIBERS AS A REINFORCEMENT IN CONCRETE

LENKA BODNÁROVÁ[a], MONIKA FIALOVÁ[b], DANIEL KOPKÁNĚ[a], TOMÁŠ MORÁVEK[b], PAVEL SŤAHEL[b], MIRKO ČERNÁK[b,c]

[a] Faculty of Civil Engineering, Brno University of Technology, Veveří 95, 662 37 Brno, Czech Republic, [b] Department of Physical Electronics, Faculty of Science, Masaryk University, Kotlářská 2, 611 37 Brno, Czech Republic, [c] Department of experimental physics, Comenius University, Mlynská Dolina F2, 842 48 Bratislava, Slovakia
bodnarova.l@fce.vutbr.cz

Keywords: fiber-reinforced concrete, polypropylene fibers, wettability

1. Fiber-Reinforced Concrete

Fiber-reinforced concrete[1] is a composite material created by connection of concrete matrix and short reinforcement elements dispersed in matrix, while fibers take up only a small part of total volume. Fibers are added to a concrete mix which contains cement, water and fine and coarse aggregate.

Plain, mass concrete has considerably high compressive strength, stiffness, but high brittleness, low tensile strength and low shearing strength. Dispersed reinforcement compensates mainly tensile stress and prevents formation of micro-cracks caused by shrinking and development of tensile cracks in structures. Adding of fiber reinforcement can reinforce the whole volume of concrete matrix, unlike classic steel bar reinforcement.

Table I
Fibers used as dispersed reinforcement in concrete[2]

Fiber type	Tensile strength [MPa]	Tensile modulus [GPa]	Tensile strain [%] (max-min)	Density [kg m^{-3}]
Asbestos	550–960	82–138	0.3–0.1	3200
Cellulose	400–620	6.9	10–25	1500
Steel	270–2700	200	2–1	7800
Poly ethylene	÷ 690	2–4	400–100	950
Poly propylene	200–750	0.8–9.8	15–10	900
Polyester	800–1300	Up to 15	20–8	1400
AR-Glass	1700	72	2	2680
Carbon	590–4800	28–520	2–1	2000

Table II
Properties of cement matrix

	Flexural Tensile strength [MPa]	Tensile modulus [GPa]	Tensile strain [%]	Density [kg m^{-3}]
Cement matrix	3.7	10–45	0.02	2500

Role of fiber reiforcement

The purpose of dispersed reinforcement is limiting formation of shrinkage cracks, increasing fracture toughness, increasing resistance to dynamic stress, increasing resistance to high temperatures – preventing explosive flaking of concrete, decreasing of wearability and potentially other special properties.

Many different types of fibers can be used as reinforcement for concrete: steel, polypropylene, glass, carbon, cellulose, polyamide, polyvinyl alcohol, aramid or nylon fibers and other fibers.

Type and material of fiber reinforcement is selected in accordance with required properties. Properties of fibers used as dispersed reinforcement for concrete are stated in Tab. I.

Use of fiber reinforcement for preventing of formation of shrinkage cracks

Fine organic and inorganic fibers (polymeric and glass) are used mainly to limit volumetric changes of cement matrix and to limit formation of cracks. In such case, concrete is reinforced with high number of fibers even if proportion of fibers is low (1 kg of polymeric fibers contains around 300 million pieces of fibers). Depending on manufacturing technology, fine polymeric fibers can be fibrillated or monofibril. Monofibril fibers are finer and therefore they are more numerous at the same weight proportion. Monofibril fibers are manufactured individually and then they are cut to required length with smooth, circular cross section. Fibrillated fiber is made from foil and then again cut to required length with rectangular cross section and more coarse surface. Because of different way of manufacture, fibrillated fibers have several times higher section, therefore the number of fibers in a weight unit is lower – several million.

Polypropylene and glass fibers are most frequently used for preventing formation of shrinkage cracks. Compared to glass based fibers, polypropylene fiber have lower values of elasticity modulus, their effect takes place in particular during first hours of setting and hardening of concrete.

Dosage of glass and polymeric fibers to prevent formation of shrinkage cracks is 0.7–1.1 kg m^{-3} of fresh concrete or mortar in accordance with recommendations of manufacturer. If fine fibers are used, it is necessary to bear in mind that workability of concrete is reduced (by ca 30–60 mm of slump).

Increase of resistance to high temperature (to prevent explosive spalling of concrete)

Increasing resistance of concrete to high temperatures is another important role of fine polypropylene fibers or other fine inorganic fibers. Explosive spalling is caused by the build-up of water vapour pressure in concrete during fire. Increased temperature causes melting of PP fibers, which opens space for expanded water vapor, which could otherwise cause cracks in concrete.

Fibers used for such purposes are mostly polypropylene (PP) and natural (cellulose).

Dosage of fine fibers to increase of resistence to high temperature and prevent explosive sparing is 0.6–2 kg m^{-3} of fresh concrete or mortar in accordance with recommendations of manufacturer.

Use of fiber reinforcement for higher strength of concrete (in particular metal fibers or polymeric – macrofibers)

Concrete reinforced with fibers shows higher toughness compared to brittle plain concrete. Fibers (certain dosage – higher volumes) influence working diagram of concrete. Higher tensile strength and slight increase of compressive strength can be observed. Fibers enable deformation of concrete and tensile stress distribution at the point of exceeding strength of concrete, even after formation of cracks. Ultimate tensile strain of fiber reinforced concrete is higher than that of plain concrete. Steel fibers are recommended particularly to increase tensile bending strength, toughness and impact strength.

Depending on recommendation of manufacturers of particular types of fibers, reinforcement fibers can be used for high strength floors, for structures, where increased water tightness and frost resistance are required, to form base layers without cracks for other special layers, for shotcrete to reduce fallout, for renovation mortars and plasters, for production of prefabricated elements, to increase impermeability of concrete or to increase resistance of concrete to fire.

Steel fibers used as dispersed reinforcement can bring following advantages:

higher tensile strength, higher transversal tensile strength and tensile bending strength

higher impact strength

resistance to formation of cracks during setting of concrete.

Most frequently used length of steel fibers is 30–55 mm. Special metal fibers of length about 12 mm are designed for high performance concrete. Section of fibers can be either circular (diameters from 0.6 to 1.4 mm), square or more often rectangular. Fibers with round section are made by means of drawing from a wire. Consequently, they are cut, ends are shaped or pressing of indents to increase bond to concrete. Steel fibers with rectangular sections are manufactured through cutting from sheet metal, often they are shaped by imprints or dents on the surface.

Consistency of steel-fiber reinforced concrete is strongly affected both by the type of steel fibers and by their weight proportion. Dosage rates of steel fibers are between 20 and 50 kg. For this reason, it is necessary to design concrete with workability about 180–200 mm of slump for preliminary tests of pumpable concrete, because addition of steel fibers decreases workability to ca 100–150 mm of slump, which is adequate for pumpable concrete.

Reinforcement with fibers (usually metal, glass or polymeric) can considerably enhance properties of concrete, however, fiber reinforcement is not designed to replace classic steel bars reinforcement.

2. Polypropylene fibers

Polypropylene is a thermoplastic polymer produced by polymerization of monomer units. Propylene, the structural unit, is containing three atoms of carbon and six atoms of hydrogen. Polypropylene, especially in the form of fibers, is widely used in many industrial applications (automotive, textile or food industry)[3].

Nowadays PP fibers are more and more used as a reinforcement in concrete due to their versatile properties such as a resistance to many chemical solvents, high melting point and low cost. The main technological problem of using PP fibers as a reinforcement is a weak adhesion between PP fibers and cement matrix, related to the hydrophobic surface of fibers. There were tested several methods of PP surface treatment that lead to the stronger bonding such as chemical, mechanical or plasma treatment[4–6].

The plasma technique is relatively new, simple and effective method of polymer surface modification. It was confirmed that the plasma treatment of polymers results in the increase of the surface energy[7–9]. In this contribution the plasma treatment by a Diffuse Coplanar Surface Barrier Discharge (DCSBD)[9] was studied.

Wetting properties of PP fibers after plasma treatment

The wetting properties of PP fibers were investigated by two methods of measuring the weight of absorbed water in bunches of PP fibers. In a first case there was measured a weight of a bunch of PP fibers before and after soaking in water. The difference between these weights gave the absorption capacity of the bunches as shown Fig. 1.

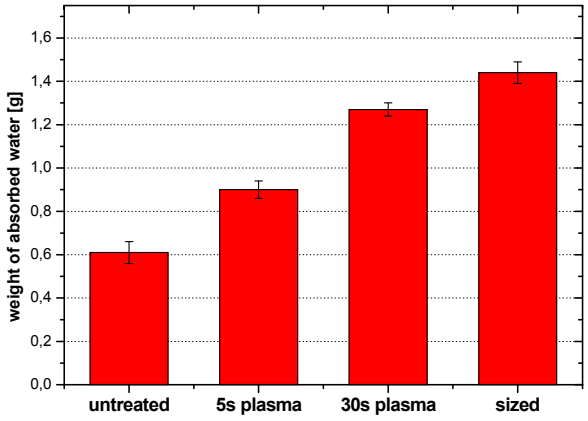

Fig. 1. **The comparison of weights of absorbed water in bunches of untreated, chemically treated and plasma treated PP fibers**

The other method is based on the measuring the weight of absorbed water as well, but the principal effect is the capillarity. The bunch of PP fibers was touching a surface of water and absorbed it. The weight of absorbed water as a function of time was measured (Fig. 2).

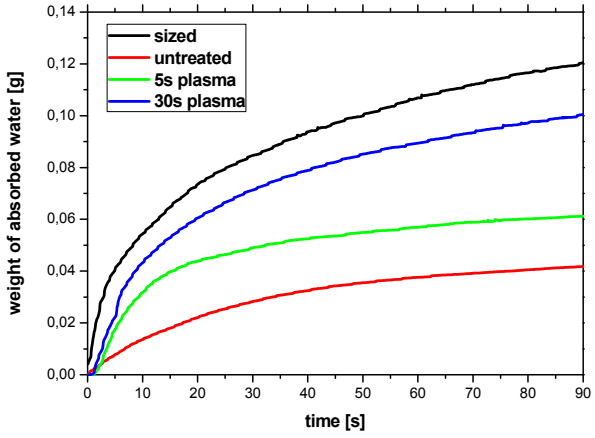

Fig. 2. **The weight of absorbed water in a bunch of untreated and treated PP fibers as a function of time**

The plasma treatment of PP fibers led to an increase of wetting properties, accordingly the water absorption of PP fibers was improved. The 30s plasma treated PP fibers absorbed twice as much water as untreated fibers and about 12% less water than sized fibers as shown Fig. 1 and Fig. 2.

3. Plasma treated PP fibers as a reinforcement for concrete

The performed test was based on testing of flexural strength in early age, mainly 12 hours after mixing. The experiment set up is based on three point test of bending flexural strength, where the test continued after the rupture of specimen until 4mm of total deflection was reached (in one minute). In this way the behavior of fibers and its effect on immature concrete can be evaluated. The Fig. 3 shows results obtained on specimens 4*4*16 cm in size. The results indicate that mixes with fibers had better performance at every level.

Table III
Composition of cement paste

Component	Mass [kg m^{-3}]	Volume [%]
Cement 32,5R	535,3	17,3
Aggregate 0-4	1472,3	55,6
Water	269,1	26,9
PP fibers	2,4	0,26

If comparing sized and plasma treated fibers the maximal strength was about the same level, while results for obtained for continuing deflection were definitely better for the plasma treated fibers. This could be explained as direct effect of change in wettability as has been discussed above.

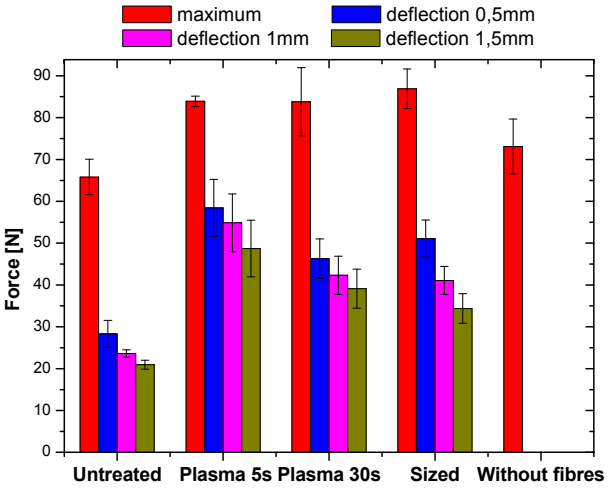

Fig. 3. **The comparison of weights of absorbed water in bunches of untreated, chemically treated and plasma treated PP fibers**

This research has been supported by the project CZ.1.05/2.1.00/03.0086 funded by European Regional Development Fund and project TA01010948 funded by Technology Agency of Czech Republic. The authors also would like to thank to KrampeHarex Company for providing PP fibers.

REFERENCES

1. Brandt A. M.: *Fibre reinforced cement-based (FRC) composites after over 40 years of development in building and civil engineering*. COMPOSITE STRUCTURES. 86 (2008).
2. 544.3R-08: *Guide for Specifying, Proportioning, and Production of Fiber-Reinforced Concrete*. ACI Committee 544.
3. William J. K., James H. H., Jefferey A. M.: *Polypropylene: Structure, Properties, Manufacturing Processes and Applications in Handbook of Polypropylene and Polypropylene Composites* (Haruhun G. K., ed.). Mercel Dekker Inc., New York 1999.
4. Pei M., Wang D., Zhao Y., Hu X., Xu Y., Wu J., Xu D.: J. Appl. Polym. Sci. 92 (2004).
5. Tu L., Kruger D., Wagener J. B., Carstens P. A. B.: Mag. Concr. Res. 50 (1998).
6. Zheng Z., Feldman D.: Prog. Polym. Sci. 20 (1995).
7. Carrino L., Moroni G., Polini W.: J. Mater. Process. Technol. 121 (2002).
8. Cui N.-Y., Brown N. M. D.: Appl. Surf. Sci. 189 (2002).
9. Šimor M., Ráheľ J., Vojtek P., Černák M.: Appl. Phys. Lett. 81 (2002).

L. Bodnárová[a], M. Fialová[b], D. Kopkáně[a], T. Morávek[b], P. Sťahel[b], and M. Černák[b,c] *([a] Faculty of Civil Engineering, Brno University of Technology, Brno, Czech Republic, [b] Department of Physical Electronics, Faculty of Science, Masaryk University, Brno, Czech Republic, [c] Department of experimental physics, Comenius University, Bratislava, Slovakia):* **Importance of Polypropylene Fibers as a Reinforcement in Concrete**

The main role of dispersed short discrete fibers as a reinforcement for concrete is to prevent formation of shrinkage cracks, their spreading in the structures and increasing resistance of concrete to high temperatures. The plasma treatment of polypropylene (PP) fibers was discussed as a method that leads to the increasing of surface freee energy of polypropylene, accordingly better adhesion between the fibers and cement matrix.

The plasma treatment improved the surface wetting properties of PP fibers. The three point bending test confirmed the improving of the mechanical performances of concrete with plasma treated fibers as a reinforcement.

Chem. Listy *106*, s1431−s1434 (2012) CEPLANT

DEPOSITION OF POLYMER FILMS ON ALUMINIUM SURFACE USING ATMOSPHERIC-PRESSURE PLASMA

LUCIA BÓNOVÁ[a]*, ANNA ZAHORANOVÁ[a], DUŠAN KOVÁČIK[a,b], MIRKO ČERNÁK[a,b]

[a] *Department of Experimental Physics, Faculty of Mathematics, Physics and Informatics, Comenius University, Mlynská dolina, 842 48 Bratislava, Slovak Republic,*
[b] *R&D Center for Low-Cost Plasma and Nanotechnology Surface Modifications, Faculty of Natural Science, Masaryk University, Kotlářská 2, 611 37 Brno, Czech Republic*
bonova@fmph.uniba.sk

Keywords: atmospheric-pressure plasma, aluminium alloy, hexamethyldisiloxane, hydrophobic film

1. Introduction

Aluminium alloys are getting renewed attention due to their light weight and high strength to weight ratios that could be transferred into higher efficiency for various technological application including aerospace, automotive, architecture and packaging. However, the corrosion of aluminium surface is a real problem. Painting and adhesive bonding of aluminium alloy are commonly used methods to prevent the aluminium surface from the corrosion. Unfortunately these methods include chemicals such as solvents and chromates. The first one is used to clean the surface from grease and dust, while chromates are used for the corrosion protection. However, plasma treatments offer an ecologically friendly alternative for cleaning and functionalizing metal surfaces.

The deposition of plasma polymerized thin-film coatings on aluminium for corrosion inhibition could provide an alternative to the conventional chromate conversion and to the wet chemistry.

Plasma polymerization is a universal method for the deposition of layers with properties useable for a wide range of applications[1]. This is caused by the high degree of control of their properties, which may be varied widely by plasma parameters. Plasma polymerized films have special advantages such as a thin film, a highly cross-linked, pinhole-free structure and in general good adhesion on substrates.

Widely used thin film material is silicon dioxide (SiO_2), which is the most common dielectric in semiconductor technology, serves as corrosion protection or permeation barrier in the packaging industry. Preparation of SiOx films by plasma enhanced chemical vapour deposition (PECVD) at low pressures has been extensively studied in the past[2,3]. Plasma polymerization of hexamethyldisiloxane (HMDSO) as monomer admixture to carrier gas seems to be very suitable for preparing thin-film coating on the surface.

In the recent years many works has been published using the radio-frequency (RF) low-pressure discharge for plasma polymerized coatings on different materials. Vasallo et al.[4] demonstrated in their work that hexamethyldisiloxane (HMDSO) layers deposited on steel exhibited good anti-corrosion properties when RF plasma discharge is fed with oxygen in addition to HMDSO. The anti-corrosion effect of organosilicon-based coatings deposited on aluminium alloy by means of a low-pressure plasma process was studied by Fernandes et al.[5] where different gases were used for HMDSO deposition process. Pre-treatment of the aluminium surface like cleaning is the important part of the polymerization process. Azioune et al.[6] investigated that the most effective way to clean the aluminium surface is pure argon plasma fed by RF discharge. Also oxygen and argon/oxygen mixtures were tested. The effectiveness of plasma cleaning was checked by means of X-ray photoelectron spectroscopy (XPS) and contact angle measurements.

Recently the attractive alternative to these low-pressure processes is the SiO_x deposition at atmospheric pressure, where no expensive vacuum pumping systems and batch processing would be necessary in a production line. Dielectric barrier discharges (DBDs) are nowadays widely used for many plasma processes such as modification of surface properties (improving wettability of polymers, adhesion properties, etc.) and also for functionalization of surfaces and plasma polymerization processes by DBDs are studied.

Plasma discharges working at atmospheric pressure like DBDs and plasma jets are suitable to treat flat surfaces. Bour et al.[7] deposited HMDSO layer on galvanized steel to give a protective coating against corrosion using DBD discharge. Plasma polymerization was carried out in different ways. To protect the aluminium from corrosion Lommatzsch et al.[8] apply an atmospheric pressure plasma jet. Also Trunec et al.[9] used a DBD discharge for HMDSO layer deposition on different materials.

2. Experimental setup

The organosilicon monomer used in this work was HMDSO (for synthesis, Merck Schuchardt OHG, Germany). As the aluminium substrates the aluminium alloy (99.5% Al) was used. To establish well defined initial conditions, before the experiment all samples were chemically pre-cleaned.

The plasma polymerization process was carried out in the plasma reactor based on the new type of surface DBD

– so called Diffuse Coplanar Surface Barrier Discharge (DCSBD)[10] – a planar source of the low-temperature plasma (Fig. 1). DCSBD plasma source generates thin (~ 0.3 mm) layer of diffuse non-equilibrium plasma of an extremely high plasma power density about 100 W cm^{-3}, which results in plasma processing times in order of one second.

The discharge was generated in the mixture of nitrogen and HMDSO. The N_2/HMDSO mixture was prepared by mixing the pure nitrogen with the nitrogen gas bubbled through liquid HMDSO monomer at 20 °C. To find suitable conditions for polymeric thin layer deposition, the ratios of nitrogen and HMDSO were experimentally tested.

The DCSBD electrodes consisting of 19 pairs of silver strip electrodes embedded 0.5 mm below the surface of 96% Al_2O_3 ceramics was energized by 14 kHz sinusoidal voltage, supplied by HV generator LIFETECH VF 700. The power supplied to the discharge was 195 W and the gap between the ceramics and sample was 0.3 mm.

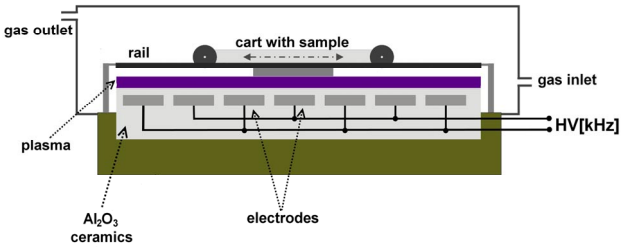

Fig. 1. **Scheme of the experimental atmospheric DCSBD plasma deposition reactor**

Contact angle measurements were carried out with Surface Energy Evaluation System (SEE System, Advex Instruments s.r.o., Czech Republic). Water drops of 2 μl were used to determine the contact angles. Each contact angle is an average of 10 measurements.

Chemical structure of the coatings was evaluated by Fourier Transform Infrared (FTIR) spectroscopy in attenuated total reflectance (ATR) using Bruker Optics Vector 22, MIRacle^{TM} spectrometer (PIKE Technologies). As the ATR crystal diamond/ZnSe was used (45° incidence angle). Data were collected from 600–4000 cm^{-1} wavelength range with 20 scans for each sample. The resolution was 4 cm^{-1}.

TOF SIMS IV (ION-TOF, Münster, Germany) spectrometer was used to measure the evidence of HMDSO layer. Measurements were carried out with a bismuth ion gun, operated at 25 keV ion energy and current 1 pA.

Measurements for the polymer layer thickness was carried out by FIB-SEM LYRA 3 GM nanotechnology workstation (TESCAN, Czech Rebublic).

Corrosion protection of HMDSO layer was tested by the immersion of aluminium samples into the 5% NaCl solution with the temperature of 35 °C and immersing time 120 h.

3. Results and discussion

To investigate the optimal deposition parameters for plasma polymerized HMDSO (pp-HMDSO) layer deposited on aluminium surface, different nitrogen and HMDSO ratios were used. The plasma polymerization process time was set to 60 sec. Table I shows results of Water Contact Angle (WCA) measurements for different HMDSO relative concentrations used in polymerization process.

Table I
Results of WCA measurements for different HMDSO relative concentrations in gas mixture of (N_2+HMDSO) measured immediately after polymerization and after 24 hours ageing

(HMDSO+N_2)/ N_2 concentration [%]	WCA immediately [°]	WCA after 24 hrs [°]
8.3	87.60 ± 3.25	100.64 ± 1.67
12.5	93.62 ± 1.29	103.25 ± 4.57
16.6	66.84 ± 1.90	81.2 ± 2.61
20.8	86.24 ± 4.22	95.97 ± 1.68
25	66.72 ± 14.94	80.94 ± 2.47

The contact angles were measured directly from the image of the solid-liquid meniscus of a liquid drop set taken with CCD camera. First measurements of WCA were taken immediately after the plasma-polymerization. Samples with deposited layer were stored on air and measured again after 24 hours ageing. These measurements indicate that the hydrophobicity still increase after the polymerization process and the most hydrophobic deposited layer is achieved at 12.5 % relative concentration of HMDSO in gas mixture.

The chemical composition analysis of the polymer film deposited on aluminium surface from mixture N_2/HMDSO was done by means ATR-FTIR. In the Fig. 2 the ATR-FTIR spectra of pp-HMDSO layer deposited on the sample for 60 sec (a), for 30 sec (b) as well as the reference sample spectrum (c) are shown. ATR-FTIR spectroscopy of the deposited pp-HMDSO layer confirms the presence of vibrational state primary amino functional groups (NH, NH_2), vibrational states of hydrogen (C-H, O-H) and also methyl groups (CH_n), generated by fragmentation of the monomer in the plasma and bounded to the surface of the aluminium substrate[11]. The IR spectrum exibits intensive absorption band at 2960 cm^{-1} and 2925 cm^{-1} which indicates the presence of CH_3 and CH_2 groups respectively. The deposited film exhibited strong absorption at 1270 cm^{-1} associated with the Si-CH_3 group. The most intensive absorption band is at 1070 cm^{-1} and peaks in this region can be interpreted as Si-O-Si, Si-CH_2-Si, Si-O-C or Si-NH-Si groups. It is clear from the Fig. 2 that longer

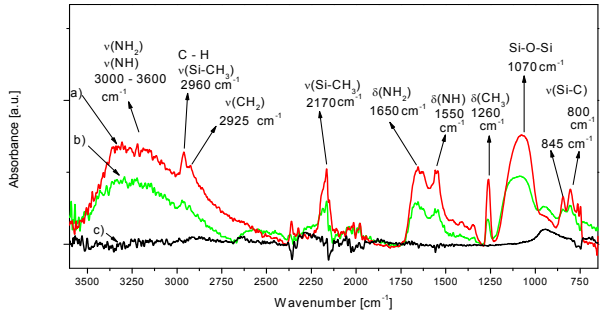

Fig. 2. **ATR-FTIR absorption spectra of: (a) pp-HMDSO – 60 s polymerized, (b) pp-HMDSO – 30 s polymerized, (c) aluminium surface – reference sample**

polymerization time brings more intensive absorption in regions denoted of HMDSO fragments bounded on aluminium surface.

The changes of the polymer film deposited on aluminium surface after the salt water test of corrosion protection were analysed by the means of FTIR also. The results are presented in Fig. 3, where chemically cleaned Al sample (d), chemically cleaned Al sample after salt water test (a), sample with HMDSO layer (c) and sample with HMDSO layer after the salt water test (b) are shown.

From analyses of the most intensive peaks in Fig. 3 is clear, that the polymer layer deposited on the aluminium surface is the same after salt test, and there is evidence of the changes on the aluminium surface. The are the most intesive peak in the region of 3000–3600 cm^{-1} , which may be assigned to –OH groups and the intensive peak at 1067 cm^{-1} which may indicate the presence of Al-O or Al-Cl group.

SIMS measurement was used to study the existence of monomer fragments in deposited film. The SIMS spectrum of pp-HMDSO coated aluminium sample is

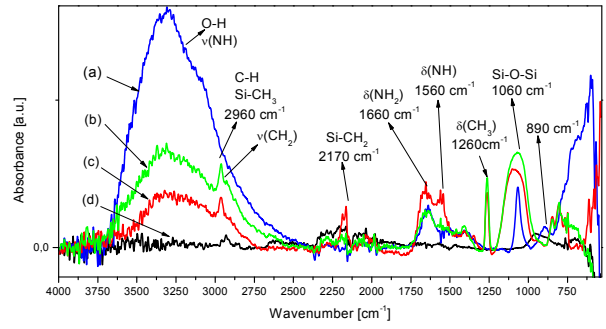

Fig. 3. **ATR-FTIR absorption spectra of: (a) chemically cleaned Al sample after salt test, (b) pp-HMDSO sample after salt test, (c) pp-HMDSO sample, (d) chemically cleaned Al sample**

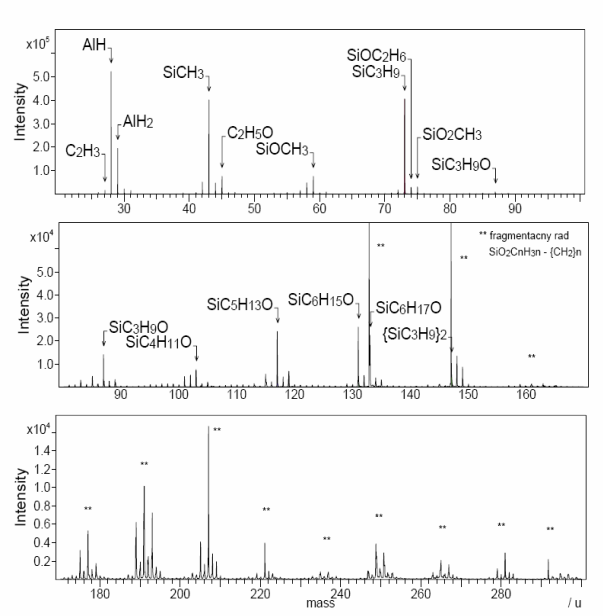

Fig. 4. **SIMS spectrum of pp-HMDSO coated Al sample**

shown in Fig. 4. As can be seen the evidence of pp-HMDSO layer was confirmed by measuring the fragmentation row of $Si\text{-}O_2\text{-}C_n\text{-}H_{3n}\text{-}\{CH_2\}_n$ and also by detection of the methyl groups bonded to Si or SiO.

To confirm the corrosion protection of pp-HMDSO layer on aluminium surface, samples were immersed in the NaCl solution for 120 h. For comparison uncoated aluminium samples were also tested. The results can be seen in Fig. 5 where the aluminium surface without protection coating and pp-HMDSO layer coated aluminium samples are shown before and after the salt test. Salt water test showed the protective effect of the pp-HMDSO layer on

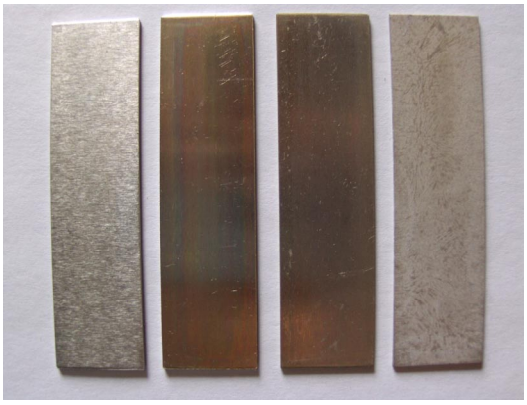

Fig. 5. **Photographs of Al samples: (a) chemically cleaned Al sample, (b) pp-HMDSO sample, (c) pp-HMDSO sample after salt test, (d) chemically cleaned Al sample after salt test**

the aluminium surface. On the aluminium surface without deposited layer there were spots of typical aluminium corrosion after immersion in the salt water.

To measure the thickness of pp-HMDSO layer the FIB-SEM was used. The surface of the sample was sputtered using gallium ion gun with accelerating voltage 30 kV. The measured pp-HMDSO layer was 250 nm.

4. Conclusion

In this paper the preliminary results of the polymer hydrophobic layer deposition on the aluminium surface were presented. The layer was deposited from the mixture of organosilicon monomer HMDSO with nitrogen using the DCSBD plasma source at atmospheric pressure. The optimal deposition time was 60 second at energy power to plasma 195 W. The polymer layer was hydrophobic with the water contact angle about 100 degrees. The FTIR spectra showed the chemical structure of the polymer layer – the presence of Si-CH_3, Si-CH_2, Si-O-Si, C-N, and O-H groups. The SIMS analyses confirmed also the fragmentation of monomer and presence of methyl groups bounded on Si or SiO. Salt water corrosion test confirmed the protection properties of polymer layer on the aluminium surface. By this manner it can be deposited on the aluminium surface the thin hydrophobic polymer layer with good adhesion to the surface and anticorrosive properties, as was demonstrated by the results of surface analyses (WCA, FTIR, SIMS, salt test).

This work is the result of the project implementation: 26240220002 and 2622020004 supported by the Research & Development Operational Programme funded by the ERDF. This work has been supported also by the project R&D center for low-cost plasma and nanotechnology surface modifications CZ.1.05/2.1.00/03.0086 funding by the ERDF.

REFERENCES

1. Cho S. H., Park Z. T., Kim J. G., Boo J. H.: Surf. Coat. Technol. *174-175*, 1111 (2003).
2. Aumaille G., Vallée K., Granier A., Goullet A., Turban F.: Thin Solid Films *359*, 188 (2000).
3. Hegemann D., Vohrer U., Oehr C., Riedel R.: Surf. Coat. Technol. *116-119*, 1033 (1999).
4. Vassallo E., Cremona A., Laguardia L., Mesto E.: Surf. Coat. Technol. *200*, 3035 (2006).
5. Fernandes J. C. S., Ferreira M. G. S., Haddow D. B., Goruppa A., Short R., Dixon D. G.: Surf. Coat. Technol. *154*, 8 (2002).
6. Azioune A., Marcozzi M., Revello V., Pireaux J. J.: Surf. Interface Anal. *39*, 615 (2007).
7. Bour J., Bardon J., Hugues A., Del Frari D., Verheyde B., Dams R., Vangeneugden D., Ruch D.: Plasma Process. Polym. *5*, 788 (2008).
8. Lommatzsch U., Ihde J.: Plasma Process. Polym. *6*, 642 (2009).
9. Trunec D., Zajíčková L., Buršíková V., Studnička F., Sťahel P., Prysiazhnyi V., Peřina V., Houdková J., Navrátil Z. and Franta D.: J. Phys. D, Appl. Phys. *43*, 225403 (8pp) (2010).
10. Šimor M., Ráheľ J., Vojtek P., Brablec A., Černák M.: Appl. Phys. Lett. *81*, 2716 (2002).
11. Milata V. et al.: *Applied Molecular Spectroscopy*, STU Bratislava, Bratislava 2008.

L. Bónová[a], A. Zahoranová[a], D. Kováčik[a,b], and M. Černák[a,b], *([a] Dep. of Experimental Physics, Comenius University, Bratislava, Slovak Republic, [b] R&D Center for Low-Cost Plasma and Nanotechnology Surface Modifications, Masaryk University, Brno, Czech Republic):*
Deposition of Polymer Films on Aluminium Surface Using Atmospheric-Pressure Plasma

The paper presents results of plasma polymerised coating deposited from the mixtures of HMDSO monomer with nitrogen on aluminium substrate using plasma reactor based on Diffuse Coplanar Surface Barrier Discharge (DCSBD). Contact angle measurement was used to investigate the optimal deposition parameters. The deposited films were characterized by FTIR and SIMS methods. The corrosion protection of the HMDSO layer was proved by salt water test.

DIAGNOSTICS OF DIFFUSE COPLANAR SURFACE BARRIER DISCHARGE OPERATED IN ARTIFICIAL AIR WORKING GAS: BASIC RESULTS

JAN ČECH*, JANA HANUSOVÁ, PAVEL SŤAHEL

R&D center for low-cost plasma and nanotechnology surface modifications, Faculty of Science, Masaryk university, Kotlářská 2, 611 37 Brno, Czech republic
cech@physics.muni.cz

Keywords: DCSBD, diffuse coplanar surface barrier discharge, time resolved, discharge pattern, spatially resolved, optical emission spectroscopy, OES, iCCD, plasma diagnostics

1. Introduction

In past decades the importance of barrier dicharges[1] as the sources of non-equilibrium plasmas for material processing has raised. With increasing demand on so called "green technologies" and low environmental footprint, low-cost plasma treatment technologies have become requested alternatives to classical chemical treatment.

The Diffuse Coplanar Surface Barrier Discharge (DCSBD) belongs to group of barrier discharges. Plasma of DCSBD is generated in thin layer[2] above dielectric at relatively high power densities of the order of 100 W cm^{-3}. The discharge consists of thin channels (filaments or microdischarges[3]) crossing the electrode gap between electrodes and visually diffuse-like layer above electrodes. These properties make DCSBD a promising candidate for high-speed plasma processing[4].

DCSBD has been successfully tested as the low-cost atmospheric pressure plasma source. DCSBD operated in ambient air at industrial production lines in continuous regime (in-line) seems to be suitable plasma source for plasma treatment of low-value-added materials[5].

To better understand the DCSBD behavior in artificial air at atmospheric pressure the spatially resolved optical emission spectroscopy (OES) and time-resolved optical imaging of DCSBD were performed. The basic results are given in presented paper.

2. Experimental setup – simplified DCSBD cell

For the study of DCSBD properties over wide range of physical conditions and discharge configurations the simplified DCSBD cell or system was developed. This setup (discharge cell) is given in Fig. 1. In Fig. 1 (left) the cross-section of discharge cell is given. The discharge cell is made of polymer capsule in which the system of semi-movable electrodes is placed. Both electrodes are pressed against dielectric plate and dipped in insulating oil bath. The arbitrary rectangular electrode gap between electrodes can be set with width up to 5 mm. The minimum distance between electrodes is governed by the insulating properties of oil bath and in present study the electrode distance was set to 0.55±0.05 mm. The maximum electrode distance is governed by power supply unit, resp. by the maximum allowable high voltage applicable to the powered electrode. In practice the limit of maximum electrode distance of described system is about 2.5 mm.

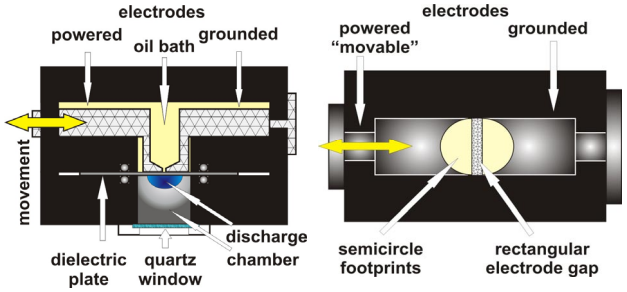

Fig. 1. **Simplified DCSBD discharge cell. Cross-section of simplified developmental DCSBD cell (left) and electrode system ground plan, with electrode gap (right) are depicted. The dimensions are not proportional**

Great advantage of the simplified DCSBD setup is the ability of easy of change of dielectric plate and electrode gap width. The dielectric plate is pressed directly to the surface of electrodes, which form two semicircle footprints on the dielectric plate, forming rectangular electrode gap in between. The schematic view of the electrodes is given in Fig. 1 (right). The view plane of the picture is the same as if the paper would be the dielectric plate. The diameter of semicircle electrodes is approx. 20 mm.

Discharge chamber is placed from the opposite side of dielectric plate; see Fig. 1 (left). The dielectric plate is made of 96% alumina (Al_2O_3) with dimensions of 10×10 cm and thickness of approx. 0.6 mm. Discharge chamber enables us to operate the discharge in controlled working gas environment. Quartz window on the opposite side of discharge chamber enables us to perform optical diagnostics of the discharge.

3. Experimental setup of time resolved iCCD imaging and spatially resolved OES, resp.

Experimental setup for time resolved iCCD measurements is given in Fig. 2. The discharge cell described in section 2 is used.

Two gas flow controllers Voghtlin Instruments red-y GCR were used to set requested working gas mixture. As primary gasses nitrogen of the purity better than 99.996 % and oxygen of the purity better than 99.996 % were used. The gas mixture ratio of nitrogen to oxygen of 80:20 was used in described experiments. The total gas flow rate was kept at 3 slpm.

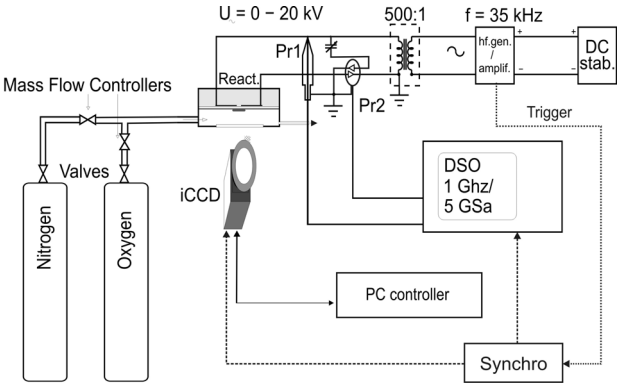

Fig. 2. **Experimental setup of time resolved iCCD imaging**

High voltage (HV) power supply was used to ignite and maintain the discharge. The HV power supply consists of high frequency tunable generator LIFETECH HF Power Source powered by stabilized DC power source STATRON 3262 and LIFETECH HV transformer. The HV power supply was operated at 30 kHz and 30 $kV_{peak\text{-}to\text{-}peak}$ for OES measurements, resp. 28 $kV_{peak\text{-}to\text{-}peak}$ for iCCD measurements, sine-wave.

The current-voltage characteristics were recorded using LeCroy WaveRunner 6100A 1 GHz/5 GSa digital storage oscilloscope coupled with HV probe Tectronix P6015A 1000:1 (in Fig. 2. Denoted as Pr1) and Pearson Current Monitor 2877 (in Fig. 2. Denoted as Pr2).

Variable high voltage capacitor was used as the displacement current compensator. The HV capacitor was connected antiparallel through current probe. Tuning the HV capacitor to the capacity close to discharge cell capacity effectively reduces measured displacement current of discharge cell which is of the same order as the discharge current. This increases effectively the signal-to-noise ratio of discharge current measurements.

For the high speed synchronized discharge imaging, the Princeton Instruments PI-MAX 1024RB-25-FG-43 iCCD camera equipped with 50 mm, f/2.8 UV lens was used. The iCCD camera was placed along axis of symmetry perpendicular to DCSBD plasma layer.

To synchronize and semi-automate the measurements, the Agilent 33220A function generator was used. As the source signal the reference signal of HF generator was used. The generator fires triggering signals for synchronous iCCD image capture together with current-voltage measurement of the same event.

This setup enables us to take series of synchronized images of the discharge together with its current-voltage characteristics with the resolution of single half-period of high voltage waveform. In presented work the 100 images series of first, second and both half-periods were taken with gate times of 17, resp. 34 μs. The iCCD delays were set in the way to guarantee that images represent all discharge events of half-periods that can be identified in current-voltage waveforms.

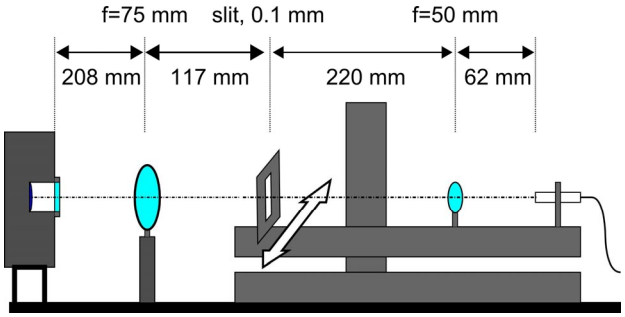

Fig. 3. **Schematic view of the optical bench system, optical parameters are marked and also the scanning direction**

Experimental setup for spatially resolved optical emission spectroscopy (OES) measurements is similar to previous one. The discharge cell and electrical parameters setups were the same as described for iCCD measurements. The experimental setup given in Fig. 2 was kept with the exception of the iCCD/optical bench system substitution.

For spatially resolved OES the computer programmed 3D stage carrying optical bench coupled to spectrometer was used instead of iCCD camera. We used 3 precision motorized linear stages Zaber T-LSQ 150 B coupled to develop XYZ-3D motion stage. The schematic view of the optical bench system is given in Fig. 3. From the left to the right the optical pathway is as follows: The image of discharge in discharge chamber is focused using fixed positioned f = 75 mm quartz lens to the entrance slit of the 0.1 mm width placed on movable bench. The spatially resolved light is then collected using f = 50 mm quartz lens and optical fiber holder. As the detector, the quartz fiber coupled spectrometer Avantes AvaSpec-2048TEC-2 with thermoelectrically cooled CCD was used. The optical resolution of spectrometer was 1.4 nm FWHM.

4. Results and discussion

In Fig. 4 the typical optical emission spectrum of DCSBD burning in the mixture of nitrogen and oxygen is given. To emphasize signal from atomic oxygen lines the spectrum with higher oxygen ratio was selected. The correction to spectrometer sensitivity was not performed in Fig. 4 to enhance readability and suppress noise and background shift in the spectrum. Dominant part of the spectra consists of molecular bands of second positive system of

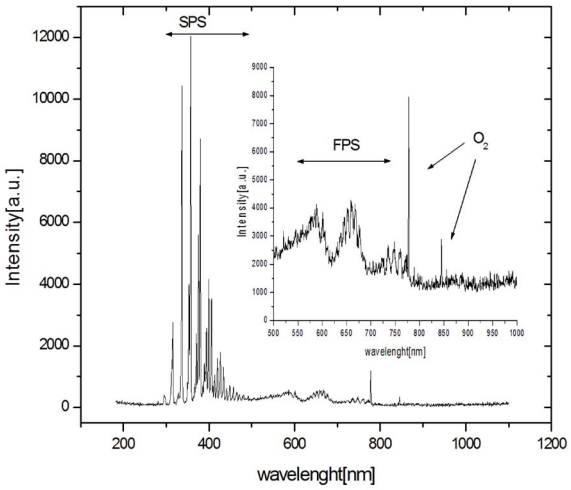

Fig. 4. **Optical emission spectrum of DCSBD near the nitrogen emission intensity maximum. The nitrogen:oxygen ratio was 20:80**

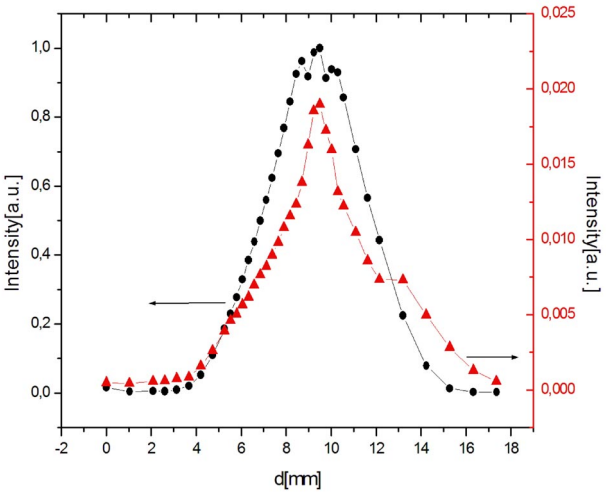

Fig. 5. **Spatial intensity profiles of nitrogen molecular band at 337.13 nm (circle symbols) and atomic oxygen triplets at 777.45 nm (triangle symbols). The distance across discharge pattern is given on the horizontal axis and it is denoted by *d***

nitrogen (SPS, $C\,^3\Pi_u \rightarrow B\,^3\Pi_g$) with maxima at 337.13 nm. At higher wavelengths the weak bands of first positive system (FPS, $B\,^3\Pi_g \rightarrow A\,^3\Sigma_u^+$) can be also identified. At wavelengths of 777.45 nm and 845.64 nm the spectrally unresolved triplets of atomic oxygen are identified. Due to limited sensitivity and spectral resolution of spectrometer other spectral systems as first negative system of nitrogen or NO-γ system (in UV range) cannot be observed.

Using the semi-automated stage with optical bench system, the spatially resolved spectral intensities can be obtained. The spatially resolved spectra were taken from approx. 1–2 mm wide zone along the horizontal diameter of the discharge pattern, distance *d* in figures, see also Fig. 7. The estimated spatial resolution is about 0.3 mm. The spatial profiles of intensities of 0-0 vibration transition of SPS of nitrogen (337.13 nm) and corresponding profile of atomic oxygen triplet intensity (777.45 nm) is given in Fig. 5. The SPS of nitrogen intensity profile has symmetrical structure with fine three-peak behavior in the middle of the discharge gap and above electrodes near gap edges. In order to confirm that this fine structure is not caused by measurement error, the comparison with independent technique (iCCD) was performed, see Fig. 8. In the profile of oxygen line emission intensity such fine structure was not observed and only one broad peak symmetrical to electrode gap position was observed.

From the SPS (vibration transitions 0-2, 1-3, 2-4 and 3-5, stopped at 380.5 nm) the vibration temperature can be estimated using the Spectrum Analyzer[6]. The spatial profile of estimated vibrational temperature is shown in Fig. 6. The estimated error is about 100 and 200 K. For comparison the nitrogen intensity profile is plotted. It can be seen, that the spatial behavior of SPS emission intensity and SPS vibration temperature is in close correlation under presented conditions. The most intensive area of the discharge is also the area of the highest vibration temperature.

The iCCD imaging was used to characterize discharge patterns of DCSBD under given conditions. In Fig. 7 the iCCD images of the discharge spatial evolution is shown. Fig. 7 contains two groups of images. In first row the images of single-shot captures of discharge patterns is given for positive (left), negative (middle) and both half-periods (right) of input HV waveform. The second row shows software accumulated images of 100 of single-shot events to emphasize the discharge pattern structures. Polarity and expected electrode/gap positions are depicted as

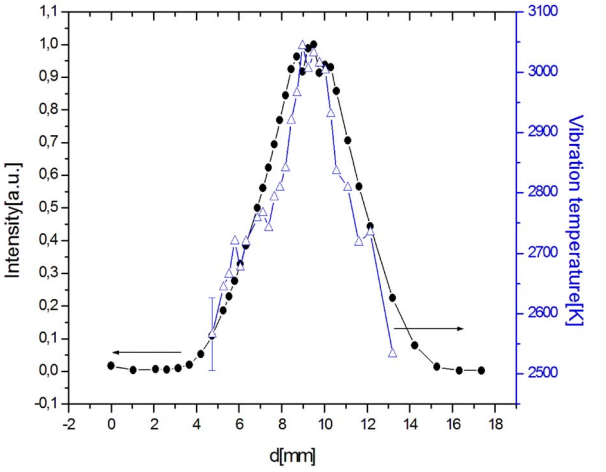

Fig. 6. **Spatial behavior of SPS intensity (circle symbols) and vibration temperature (triangle symbols) shows high spatial correlation. The distance across discharge pattern is given on the horizontal axis and it is denoted by *d***

dotted curves. Polarity is taken as polarity of HV signal on the left electrode, see Fig. 1 and 2. The discharge burns in numerous micro-discharges[3] spread along discharge gap.

To be able to compare the iCCD imaging results with the results obtained using spatially resolved OES, the image intensity calculations from similar discharge area were performed. The results are given in Fig. 8. For both half-period curve one can see the same spatial structures as in curve representing nitrogen emission intensity. This is in agreement with the spectral intensities of the discharge and spectral response of iCCD camera intensifier stated by the manufacturer.

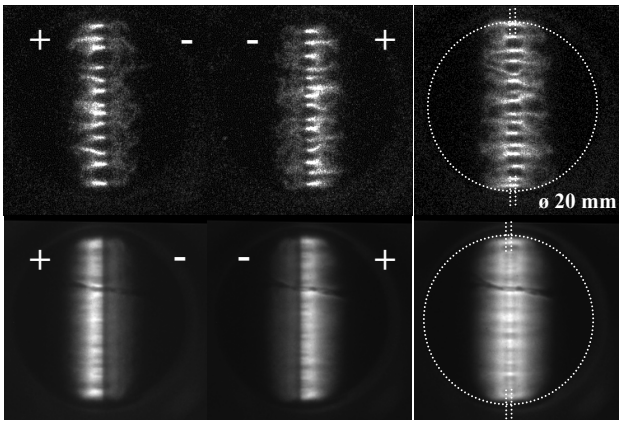

Fig. 7. **iCCD images of DCSBD. From the left to right: positive, negative and both half-periods are given. First row shows selected single-shot images, second row represents sum of 100 of single images. The dark artifact in upper third of images was related to dielectric plate artifact. The input voltage of 28 kV_{pp} was used**

5. Conclusion

In this paper we have presented optical measurements of DCSBD in artificial air. The close correlation of spatial profiles of vibration temperature estimated from SPS of nitrogen with spatial profile of SPS intensity was presented. It was shown that the SPS intensity has a fine spatial structure above electrode gap, while the oxygen triplet profile has a single peak behavior. The fine structure of SPS intensity profile was confirmed using time resolved optical imaging (iCCD). This fine structure can be reconstructed using accumulated intensity profiles of positive and negative half-period that have double-peak intensity behavior.

This research has been supported by the project R&D center for low-cost plasma and nanotechnology surface modifications CZ.1.05/2.1.00/03.0086 funded by European Regional Development Fund and projects No. TA01011356/2011 and TA01010948/2011 of the Technology Agency of the Czech Republic.

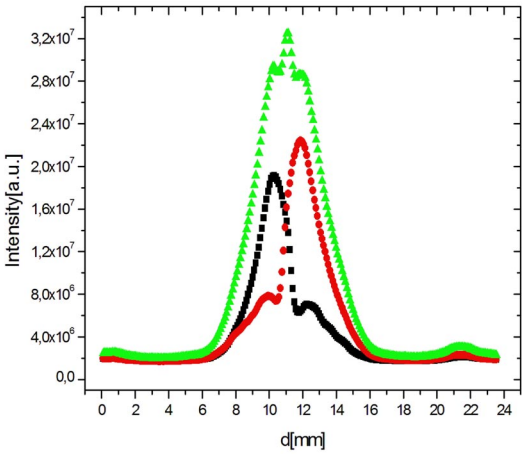

Fig. 8. **Integrated intensity profiles along horizontal diameter of discharge pattern. Curves are calculated from the sum of 100 of discharge pattern images (see Fig. 7). Positive, negative and both half-periods are depicted using square, circle, resp. triangle symbols. The distance across discharge pattern is given on the horizontal axis and it is denoted by *d*. The input voltage of 28 kV_{pp} was used**

REFERENCES

1. Kogelschatz U.: Plasma Chem. Plasma Process. *23*, 1 (2003).
2. Čech J., Hoder T., Buček A., Ráheľ J. Černák M.: *17th Symposium on Application of Plasma Processes*, 145–146 (2009).
3. Hoder T., Brandenburg R., Basner R., Weltmann K.-D., Kozlov K.V. and Wagner H.-E.: J. Phys. D, Appl. Phys. *43*, 124009 (8pp) (2010).
4. Černák M., Kováčik D., Ráheľ J. Sťahel P., Zahoranová A., Kubincová J., Tóth A., Černáková Ľ.: Plasma Phys. Control. Fusion *53*, 124031 (8pp) (2011).
5. Černák M., Černáková L'., Hudec I., Kováčik D., Zahoranová A.: Eur. Phys. J.: Appl. Phys. *47*, 22806 (2009).
6. Navrátil Z., Trunec D., Šmíd R. and Lazar L.: Czech. J. Phys. *56*, Suppl. B, B944-951 (2006).

J. Čech, J. Hanusová, and P. Sťahel, *(Masaryk University, Brno, Czech Republic):* **Diagnostics of Diffuse Coplanar Surface Barrier Discharge Operated in Artificial Air Working Gas: Basic Results**

In this paper we present measurements of DCSBD in artificial air. Simplified DCSBD cell with one electrode pair with electrode gap width 0.55±0.05 mm was used. Discharge was driven using high voltage sine-wave generator at 30 kHz and 28, resp. 30 kV_{pp}. Spatially resolved optical emission spectroscopy and time-resolved optical imaging was performed. Close correlation of spatial profiles of vibration temperature of SPS of nitrogen with spatial profile of SPS intensity was presented. SPS intensity shows fine spatial structure above electrode gap, while oxygen triplet profile has only single peak behavior. The fine structure was confirmed using time-resolved optical imaging.

IMPROVEMENT OF SURFACE PROPERTIES OF REINFORCING POLYPROPYLENE FIBRES BY ATMOSPHERIC PRESSURE PLASMA TREATMENT

MONIKA FIALOVÁ[a]*, DANA SKÁCELOVÁ[a], PAVEL SŤAHEL[a], MIRKO ČERNÁK[a,b]

[a] Department of Physical Electronics, Faculty of Science, Masaryk University, Kotlářská 2, 611 37 Brno, Czech Republic, [b] Department of experimental physics, Comenius University, Mlynská Dolina F2, 842 48 Bratislava, Slovakia
mfialova@mail.muni.cz

Keywords: DCSBD, polypropylene fibre, wettability, fibre-reinforced concrete, contact angle measurement

1. Introduction

Mechanical properties as toughness, tensile strength and flexural ductility[1] of concrete can be significantly improved with addition of polypropylene fibres. For this purpose low density polypropylene is typically used. The advantage of PP fibres is their low cost and chemical stability. However, their surface energy is low. Because of hydrophobic properties of PP fibres the adhesion to cement matrix is very low and it is difficult to distribute fibres uniformly in matrix. The modification of the PP fibre surface can achieve higher wettability. There are several ways of increasing the surface energy of PP fibres: mechanical, chemical or plasma treatment[2,3]. In the first case the surface of PP is mechanically roughened, however, this modification negatively affects the mechanical properties. The chemical modification is widely used in the industry[4]. This technology is based on the surfactants which are deposited on the surface of PP and make the surface wettable. The disadvantage of this method is its instability in contact with water (the surfactants are washed away) and also it is necessary to use chemicals which are restricted by the EU legislative REACH. The method based on cold plasma treatment creates reactive hydrophilic group on the surface of PP fibres whereas bulk properties of fibre remain unchanged. Various low pressure plasma sources for treatment of PP fibres have been widely studied[3,5], however, using the low pressure plasma technologies is limited because of the necessity of expensive vacuum systems and high energy consummation. Plasma technologies operating at atmospheric pressure provide a simple low-cost technique compared with the low pressure plasmas. The dielectric barrier discharge (DBD) technology is one of the most used methods to generate cold atmospheric pressure plasma[6].

In this paper the plasma treatment of polypropylene fibres in Diffuse Coplanar Surface Barrier Discharge (DSCBD) operated at atmospheric pressure was investigated. DCSBD was developed at the Masaryk University in Brno and Comenius University in Bratislava[7–9].

This type of discharge is featured by high electron temperature, however, rotational temperature is close to room temperature. Due to high non-isothermicity of discharge it has a great potential for industry plasma treatment of thermal sensitive material such as polymers, paper, wood or felt[10,11].

2. Experimental setup

DCSBD operated at atmospheric pressure was used for plasma treatment of polymer fibres. Fig. 1 shows the electrode configuration of DCSBD. The electrodes are created by 32 parallel metallic strips embedded in Al_2O_3 ceramic. Thin film of macroscopically diffuse atmospheric pressure non-equilibrium plasma is created on the surface of the electrode. An image of the DCSBD plasma is shown in Fig. 2.

Plasma treatment of polypropylene fibres was carried out in ambient air. We tested the effect of plasma treat-

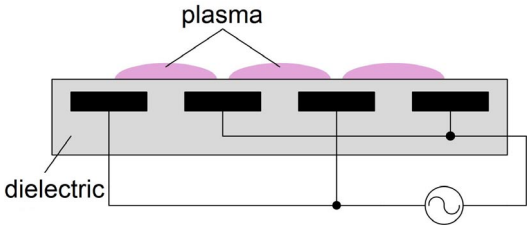

Fig. 1. **Cross-section of the discharge electrode system**

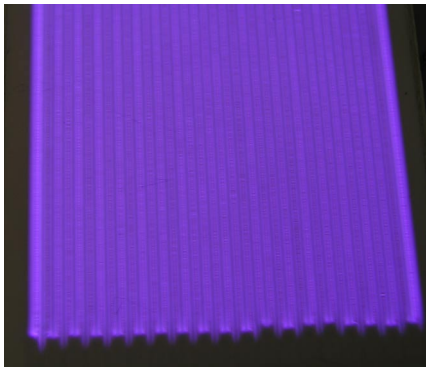

Fig. 2. **Image of thin film of DCSBD plasma**

ment on fibres for discharge power in range 250–400 W and treatment time in range 5–30 s. A high frequency voltage (14 kHz, 13 kV peak to peak) was applied between the electrodes.

Polypropylene fibres commercially produced by KrampeHarex company were used as samples[12]. The diameter of fibres with round cross section was 32 μm (±10 %), the density of fibres was 910 kg m^{-3} and tensile strength was 300 N mm^{-2} (±15 %) .

The effect of the plasma treatment on surface properties of the fibres was studied by contact angle measurement using Surface Energy Evaluation System (SEE System) made by Advex Instruments[13]. Distilled water was used as a testing liquid.

Wetting properties of treated and untreated fibres were investigated by water absorption measurement method. For this purpose 20 cm long bunch of PP fibres was used. The bunch of fibres was weighed before and after the soaking with water for 10 s. The difference of the weight of fibres after and before soaking with water gave absorption capacity of the bunch of fibres. This simple experiment shows how water absorption capacity and wetting properties of PP fibre changes after the plasma treatment.

The surface morphology was studied by stereo microscope LEICA S6 D with maximum resolution 432 lp/mm and magnification 80×.

3. Results

An image of the water drop on PP fibre before and after plasma treatment is shown in Fig. 3. The water contact angle of untreated fibre (110°) decreased to about 50° after the 30 s of the plasma treatment. This effect can be related to the formation of functional polar groups and radicals on the PP surface after plasma treatment.

Fig. 4 shows, the wettability of PP fibres increased with treatment time for four discharge power (250, 300, 350, 400 W). Water absorption of fibre increased during the first 15 s of plasma treatment, above 15 s remained constant. Moreover maximum water absorption capacity was depending on plasma power density and it increased with increasing power density.

The washing out resistance of plasma treated fibres was also investigated. Plasma treated fibres were soaked with water for 10 s, than samples were dried and consequently characterised by water contact angle measurement. The change of wettability and contact angle was measured.

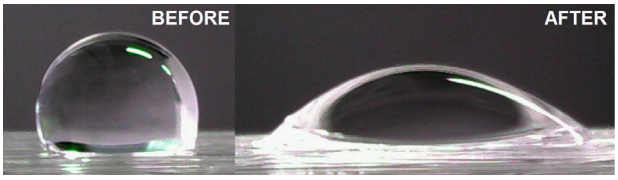

Fig. 3. **The water contact angle before and after 30 s plasma treatment at 300 W discharge power**

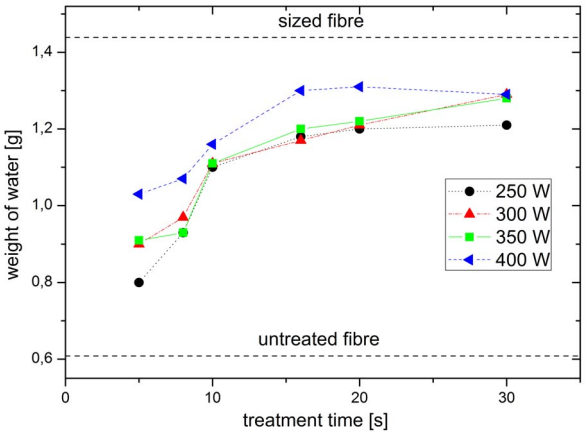

Fig. 4. **Weight of absorbed water in bunch of PP fibres as a function of plasma treatment time for different discharge power. There are marked also the values of weight for sized and untreated fibres**

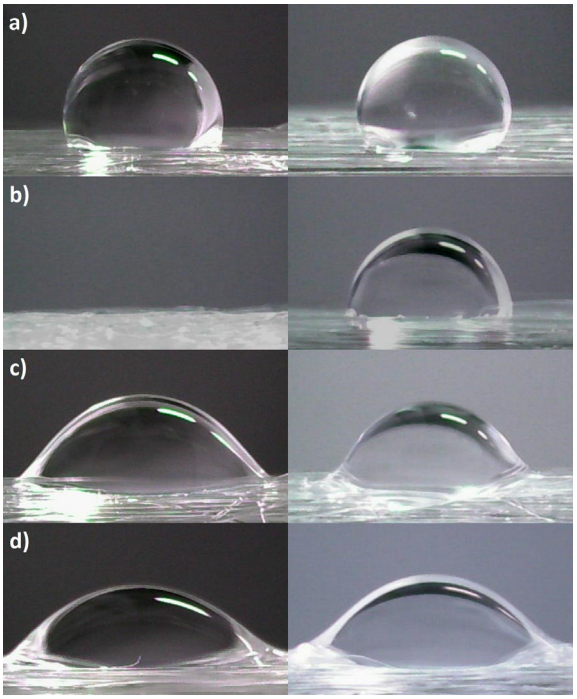

Fig. 5. **Comparison of wettability of a) untreated, b) sized and c) 5 s and d) 30 s plasma treated fibres in a left column and effect of washing out in right column. The discharge power was 300 W**

It was proven that the effect of plasma treatment was resistant to washing out in contrast to the commercial size. Soaking with water did not influence the wettability of plasma treated fibres. Commercially produced sized fibres

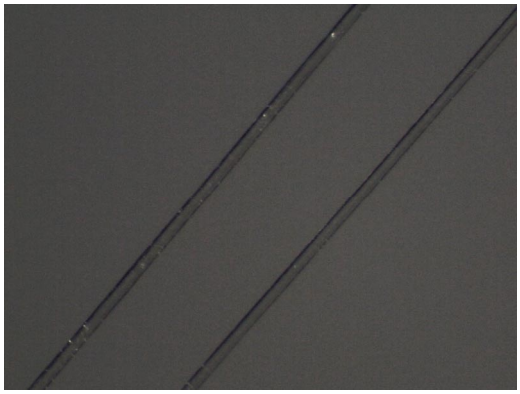

Fig. 6. **Stereo microscope image of as-received untreated fibres**

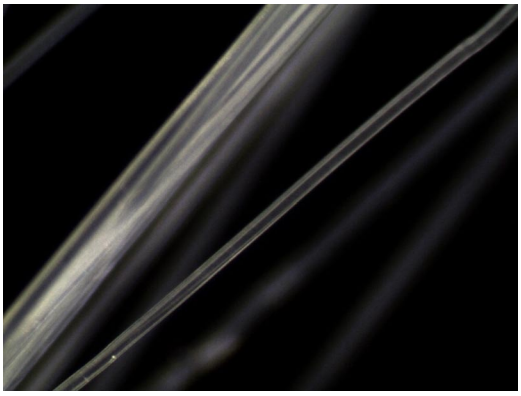

Fig. 8. **Stereo microscope image of 30 s plasma treated fibres. Discharge power was 300 W and treatment time 30 s**

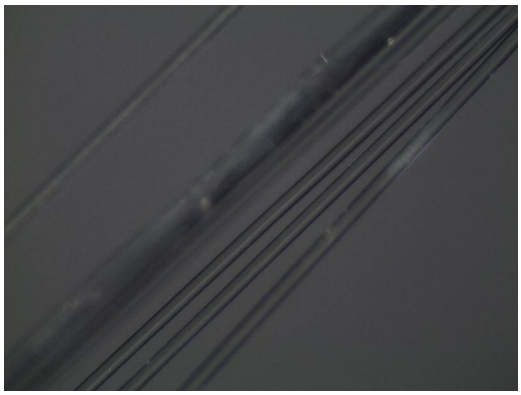

Fig. 7. **Stereo microscope image of plasma treated fibres. Discharge power was 300 W and treatment time 5 s**

were totally wetted, but after soaking with water the fibre became hydrophobic almost as untreated fibres (see Fig. 5).

The influence of plasma treatment on the surface appearance of PP fibres was studied by stereo microscope. In Fig. 6 two untreated PP fibres are shown. Plasma treatment did not affect the surface structure of PP fibre (see Fig. 7 and Fig. 8). During plasma treatment no macroscopic mechanical damage was observed.

4. Conclusion

The influence of plasma treatment on the wetting and surface properties of polypropylene fibres was investigated.

The plasma treatment of PP fibres by DCSBD led to an increase of the wettability, accordingly the water absorption of fibres improved. The surface morphology remained unchanged.

Commercially produced sized PP fibres were totally wetted, but after soaking with water the surfactants were washed out and PP fibre became hydrophobic. Plasma treated fibres exhibited washing out resistance in contrast with the sized PP fibres.

This research has been supported by the project CZ.1.05/2.1.00/03.0086 'R&D center for low-cost plasma and nanotechnology surface modifications' funded by European Regional Development Fund and by the project TA01010948 funded by Technology Agency of Czech Republic. The authors also would like to thank to KrampeHarex Company for providing polypropylene fibres.

REFERENCES

1. Shi C., Mo Y. L.: *High-Performance Construction Materials – Science and Applications*, p. 91–154, World Scientific Publishing Co. Pte. Ltd., Singapore 2008.
2. Wei Q. F.: Mater. Charact. *52*, 231 (2004).
3. Felekoglu B., Tosun K., Baradan B.: J. Mater. Process. Technol. *209*, 5133 (2009).
4. Garbassi F., Morra M., Occhiello E.: *Polymer surface: from physics to technology*, J. Wiley, Chichester 1998.
5. Wu H.-Ch., Li V. C.: Cem. Concr. Compos. *21*, 205 (1999).
6. Ma Z., Qi H.: Surf. Coat. Technol. *201*, 4935 (2007).
7. Šimor M., Ráheľ J., Vojtek P., Brablec A., Černák M.: Appl. Phys. Lett. *81*, No. 15 (2002).
8. Černák M., Černáková L., Hudec I., Kováčik D., Zahoranová A.: Eur. Phys. J.: Appl. Phys. *47*, 2 (2009).
9. http://gimmel.ip.fmph.uniba.sk/treaters/
10. Černák M.: Method and apparatus for treatment of textile materials. US Patent Appl. No. 2004/0194223, 07 October 2004.
11. Černák M.: An apparatus and method for improving felting properties of animal fibres by plasma treat-

ment. CZ Patent Appl. No. 2009/000123.
12. http://www.en.krampeharex.com/
13. http://www.advex-instruments.cz/

M. Fialová[a], D. Skácelová[a], P. Sťahel[a], and M. Černák[a,b] *([a] Department of Physical Electronics, Faculty of Science, Masaryk University, Brno, Czech Republic, [b] Department of experimental physics, Comenius University, Bratislava, Slovakia):* **Improvement of Surface Properties of Reinforcing Polypropylene Fibres by Atmospheric Pressure Plasma Treatment**

Activation polypropylene (PP) fibres used for reinforcement of concrete was tested in atmospheric pressure Diffuse Coplanar Surface Barrier Discharge generated in ambient air. The surface properties and wettability were studied by contact angle measurement and amount of absorbed water measurement. Surface morphology was investigated by optical stereo microscope.

The plasma treatment changed totally hydrophobic surface of untreated PP fibres with water contact angle about 110° to hydrophilic surface with contact angle of about 50°. In comparison with sized fibres plasma modification was resistant to washing out. The plasma treatment improved surface wettability without any macroscopically observable mechanical damage of PP fibres.

Chem. Listy *106*, s1443−s1446 (2012) CEPLANT

SOME ASPECTS OF UNDERWATER DISCHARGE GENERATED BY HV PULSES AT ATMOSPHERIC PRESSURE

OLEKSANDR GALMIZ*, ANTONÍN BRABLEC, ZDENĚK NAVRÁTIL

Dep. of Physical Electronics, Faculty of Science, Masaryk University, Kotlářská 2, 61137 Brno, Czech Republic
oleksandr.galmiz@gmail.com

Keywords: underwater discharge, OES, HV pulses

1. Introduction

Underwater electrical discharge systems attract attention of many research groups mainly for their proven efficiency in the wastewater remediation[1]. A recently emerged application for underwater discharge offering substantial economical and environmental benefits compared with conventional wet chemical methods is the surface functionalization of textile materials[2]. So far, only a small number of works has been published about diagnostics of the discharge itself due to the main concern for material treatment[3,4] and also due to the complicated nature of filamentary underwater plasma.

Surface modification of textile materials extends over a wide range of alterations to provide the desired single or multi-features for various applications. It is a highly focused area of research in which alterations to physical and/or chemical properties lead to new textile products that provide new applications or satisfy specific needs. These processes can involve numerous chemicals, some of which are toxic to humans and hazardous to the environment. In an effort to eliminate these harmful chemicals and waste products, surface modification and finishing via plasma treatment has become an attractive alternative.

As discussed in (ref.[5]), polypropylene (PP) is being increasingly used for industrial applications thanks to its beneficial properties and ability to be recycled. However, PP has a very low surface free energy, resulting in poor wettability and bonding strengths. To overcome this shortcoming, various techniques have been employed to modify the surface of polypropylene materials[6–8]. Plasma treatment is one of the most important surface modification techniques and has proven to be an environmentally friendly technique in the textile industry.

Investigation of underwater discharges generated in water solutions at atmospheric pressure has shown effective production of OH radicals, solvated electrons and a number of others active species[9,10]. This primary source of radicals is often localised in a small region related to the size of the plasma discharge. Those radicals are highly reactive. Their oxidation potentials are one order of magnitude higher than usual chemical substances used to sterilise or to remove pollutants from the liquid phase.

Electrical breakdown in liquids is generally preceded by events called streamers. The two possible mechanisms for streamer initiation need to be considered: the first is due to electron avalanche which cause electrons to be injected in the liquid and drift to the cathode, and the other is due to the formation of micro-bubbles which cause gaseous cavities to be formed that give rise to electrical breakdown in the gas bubbles. The electric field around the electrode, or the streamer channel, is highly increased, which causes an intense field emission current that eventually vaporizes the water. Streamer discharge phenomena in water are known to be influenced by various factors, such as gap geometry, water conductivity, pulse duration and amplitude of the applied voltage[11].

While in other contributions published in this issue we deal with surface treatments of PP textile as well as with binding of various atoms on the surface, in this article we studied an application of optical emission spectroscopy (OES) which has been usually used as a standard method making it possible to estimate basic parameters of plasma discharges. However, it is also a well known fact, unfortunately, that an accuracy of this method is not too high. This is also the case of the underwater discharge generated by HV pulses at atmospheric pressure when low intensity of emitted light and simultaneously high electrical interferences from the discharge reduce the chance to estimate these plasma parameters with reasonable accuracy. On the other hand OES remains the only one method due to small volume of generated plasma.

2. Experimental setup

The underwater plasma treatment was performed using two versions of experimental arrangement: single diaphragm (SD) discharge and double diaphragm (DD) discharge as illustrated in Fig. 1. The discharge was generated between two metallic electrodes at 2 cm mutual distance, the electrodes were connected to a pulsed HV power supply based on the double rotating spark gap. The maximum peak voltage was 30 kV DC and the maximum repetitive rate of pulses was 60 Hz. The propagation of discharge filaments could be influenced by parameters such as voltage, water conductivity, etc. In this case distilled water was used as a working medium. The electrodes and the slit (diaphragm) were positioned under the water level. The water conductivity range was from 0.5 to 3.7 mS cm^{-1}. A more detailed description of the experimental set-up can be found in (ref.[5]).

The discharge was studied with optical emission spectroscopy of the light coming from a narrow discharge region between the electrodes. The spectra were measured

by means of HR640 spectrometer, Jobin – Yvon (grating 1200 grooves, focal length 640 mm, CCD detector cooled by nitrogen). Molecular spectra bands of CN violet system ($B\ ^2\Sigma^+ \rightarrow X\ ^2\Sigma^+$, $\Delta v = 0$) were used for determination of vibrational temperature. H_α line profile was used to determine electron temperature and density based on tables calculated by (ref.[13]).

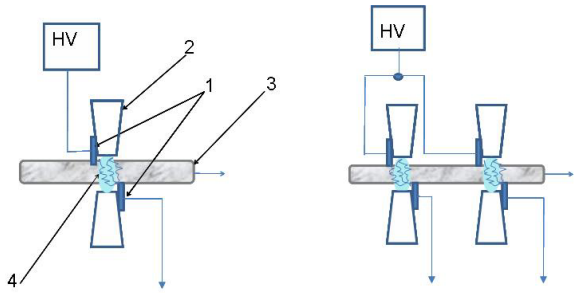

Fig. 1. **SD discharge (left) and DD discharge (right):** 1 – electrodes; 2 – diaphragm; 3 – polypropylene nonwoven fabric; 4 – discharge

The discharge was generated using a diaphragm electrode, where a narrow slit of 0.1×1×40 mm was positioned between two metallic electrodes at 2 cm mutual distance. The arrangement for double diaphragm is similar with the single diaphragm, but in this case we have two diaphragms in the same basin, the material undergoing two successive treatments. The distance between the diaphragms is 13 cm. Polypropylene nonwoven fabric of 50 gsm (grams per square meter) and 30 mm width was used for this experiment.

To keep optimal characteristics of the discharge the current and voltage measurements were done using the LeCroy WaveRunner 6100A Oscilloscope.

We performed standard Optical Emission Spectroscopy (OES) to check the plasma discharge by means of the plasma parameters[12]. The spectra profiles were measured by means of the Triax HR550 spectrometer, Jobin – Yvon (grating 1200 grooves, focal length 550 mm, CCD detector cooled by Peltier). The procedure presented in (ref.[3]), which takes into account the impact broadening by electron and quasi-static broadening by ions, in combination with new data for H_α line profile[13] was used to determine electron temperature and density. The typical profile of H_α is shown in Fig. 3.

3. Results and discussion

The typical spectrum is shown in Fig. 2 while the isolated hydrogen (H_α) and CN ($B\ ^2\Sigma^+ \rightarrow X\ ^2\Sigma^+$, 0-0) are displayed in Fig. 3 and 4, respectively.

The intensity of CN ($B\ ^2\Sigma^+ \rightarrow X\ ^2\Sigma^+$, 0-0) vibrational band and hydrogen (H_α) line vs. discharge voltage are displayed in Fig. 5. The intensity of CN band is decreasing with increasing applied voltage, in contrast with H_α. This

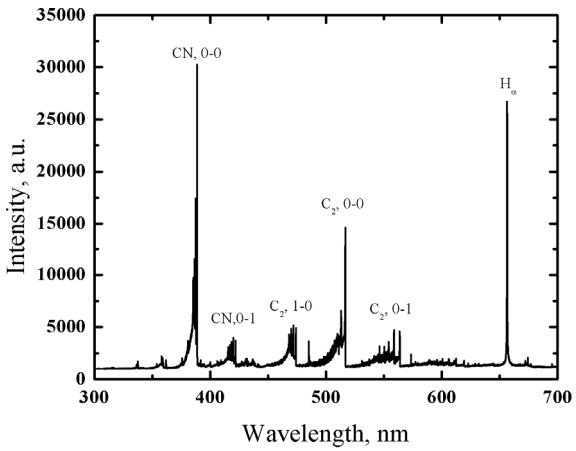

Fig. 2. **Typical spectrum of the discharge recorded in the visible range**

can be attributed to the observation, that the filaments became brighter and longer with increasing voltage in the interelectrode region. It was also found that the temperature depends significantly on conductivity as shown in Fig. 6.

The vibrational temperature estimated from CN bands remains approximately the same with increasing voltage, whereas increasing the water conductivity causes substantial rise of vibrational temperature.

The electron density changes from $1{\cdot}10^{22}$ m^{-3} to $2{\cdot}10^{24}$ m^{-3} while the electron temperature was practically constant $4{\cdot}10^4$ K in all experimental conditions studied. The error of the measured electron density was less than 5 %. The error of electron temperature was much higher, which is due to the weak dependence of the line profile on the electron temperature.

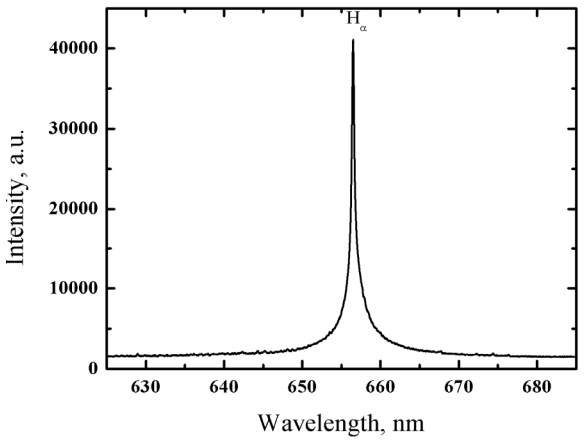

Fig. 3. **An example of hydrogen line used for the estimation of electron number density**

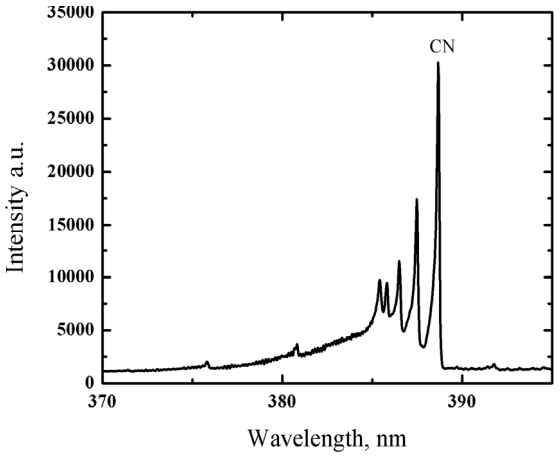

Fig. 4. **A typical example of CN (B $^2\sum^+ \rightarrow$ X $^2\sum^+$, 0-0) molecular band in case of double diaphragm discharge**

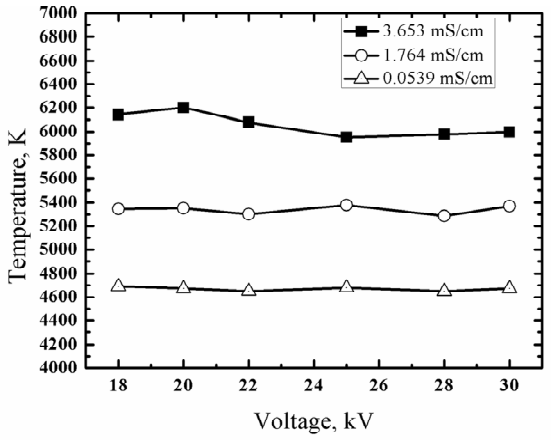

Fig. 6. **Temperature vs voltage and conductivity for double rotating spark gap and different conductivity**

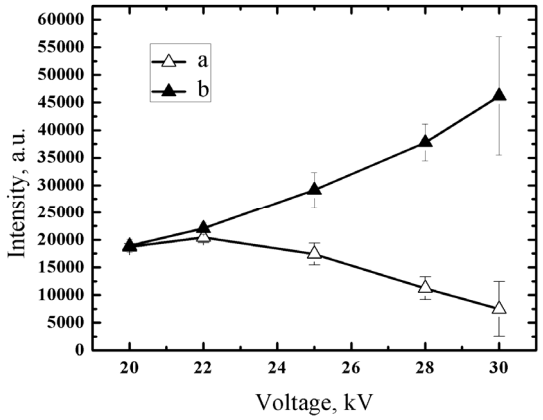

Fig. 5. **Intensity of selected components in OES spectra versus applied voltage for HV power supply based on double rotating spark gap:** a) selected CN vibrational band, b) H_α line profile

Note that presented results must be taken for preliminary ones although a characteristic data set was at disposal and individual data were obtained with reasonable precision (see above). However, individual graphs presented in Fig. 5 appear surprising and it is evident that the suggested relationship to the structure of filaments does not explain completely the origin of this phenomenon. On the other hand, the intensity of the hydrogen line is proportional to the concentration of excited atoms while the intensity of the molecular band reflects the concentration of CN molecules in concrete vibrational state and both intensities depend nonlinearly on voltage. Therefore, it could reflect nonisothermic behaviour of the discharge.

4. Conclusion

In this contribution, OES is used in order to characterize the underwater plasma discharge generated by HV pulses at atmospheric pressure. Although the knowledge of these plasma parameters does not play a dominant role in comparison with those characterizing qualities of an surface treatment by plasmas the study is very important for finding main processes running in the plasma and for determination of appropriate quantity (or quantities) making it possible, in this way, to keep the discharge in an optimal regime.

This research has been supported by OP RDI CZ.1.05/2.1.00/03.0086 funding by the Ministry of Education of the Czech Republic.

REFERENCES

1. Locke B. R., Sato M. et al.: Ind. Eng. Chem. Res. *45*, 882 (2006).
2. Pastore Ch. M., Keikens P.: *Surface characteristics of fiber and textile. Surface science series*. *b94*, New York – Basel 2001.
3. Brablec A., Slavicek P., Stahel P., Cizmar T., Trunec D., Simor M., Cernak M.: Czech. J. Phys. *52* Suppl. D 491 (2002).
4. Simor M., Krump H., Hudec I., Rahel J., Brablec A., Cernak M.: Acta Physica Slovaca *54*, 43 (2004).
5. Neagoe G.: *PhD Thesis*. Masaryk University, Brno 2011.
6. Slobodskoi S. A. et al.: Vopr. Technol. Ulavlivania i Pererab. Prod. Koksovania, *1978*, 71.
7. Sharma A. K., Locke B. R., Arce P., Finney W. C.: Hazard. Waste Hazard. Mater. *10*, 209 (1993).

8. Grimonpre D. R., Sharma A. K., Finney W. C., Locke B. R.: Chem. Eng. J. *82*, 189 (2001).
9. Sunka P., Babicky V., Clupek M., Lukes P., Simek Schmidt J., Cernak M.: Plasma Sources Sci. Technol. *8*, 258 (1999).
10. Lukes P.: *Ph.D. Thesis*, Institute of Plasma Physics, Prague 2001.
11. Bruggeman P., Leys C., Vierendeels J.: J. Phys. D: Appl. Phys. *40*, 1937 (2007).
12. Bruggeman P., Verreycken T., Gonzalez M. A., Walsh J. L., Kong M. G., Leys C., Schram D. C.: J. Phys. D: Appl. Phys. *43*, 124005 (2010).
13. Gigosos M. A., Gonzalez M. A., Cardenoso V.: Spectrochim. Acta, Part B *58*, 1489 (2003).

O. Galmiz, A. Brabec, and Z. Navrátil *(Dep. of Physical Electronics, Faculty of Science, Masaryk University, Brno, Czech Republic):* **Some Aspects of Underwater Diaphragm Discharge Generated by HV Pulses at Atmospheric Pressure**

Underwater diaphragm discharge generated by HV pulses at atmospheric pressure has been studied by OES to estimate basic plasma parameters such as electron density and temperature of excited species for various experimental conditions. It was found that intensity of emitted H_α as well as temperature depends significantly on voltage and conductivity.

CHEMICAL ASPECTS OF STREAMER MECHANISM FOR NEGATIVE CORONA DISCHARGES

JURAJ HALANDA*[a], ANNA ZAHORANOVÁ[a], JOZEF KÚDELČÍK[b], MIRKO ČERNÁK[a,c]

[a] *Dep. of Experimental Physics, Comenius University, Mlynská dolina F2, 842 48 Bratislava, Slovak Republic,* [b] *Dep. of Physics, Faculty of Electrotechnical Engineering, University of Žilina, Univerzitná* 8215/1, *010 26 Žilina, Slovak Republic,* [c] *R&D Center for Low-Cost Plasma and Nanotechnology Surface Modifications, Faculty of Science, Masaryk University, Kotlářská 2, 611 37 Brno, Czech Republic*
juraj.halanda@gmail.com

Keywords: negative corona discharge, streamer mechanism

1. Introduction

When a sufficiently high negative voltage is applied to the point of a point-to-plane electrode system at pressures above of same 10 kPa, a negative corona discharge appears at the point cathode (see Fig. 1a), where the discharge current consists of the negative corona Trichel pulses (TPs, see Fig. 1b). Each TP is discerned by a peaked signal where in several nanoseconds the current rise to a maximum of (~ $1–10^2$ mA) before decreasing to a subsequent transient glow discharge stage[1–3]. As documented in refs.[1–4], quite surprisingly such peaked signal does not significantly depend on the secondary electron emission coefficient of the cathode material used. Typically, for any form of corona discharges, the interelectrode gap can be divided to a narrow (~ 0.1–1 mm, see Fig. 1a) visible ionization region and a dark low field drift region connecting the ionization region to with the low-field passive electrode.

The TP negative corona discharges operating in ambient air are widely used in electrostatic applications (corona precipitators, separators, and powder coating systems) as a simple source of negative ions. Also, chemical reactions both in corona exposed gases[5–14] and on surfaces[14–20] have been studied rather extensively. However, despite widespread use of the TP coronas, there is no reliable and generally accepted theoretical model of this phenomenon.

2. Models of Trichel pulses formation

The model of TPs formation, which is up to the present time most commonly used in engineering including the "chemical" applications, was developed by Loeb[21] and extended by Alexandrov[22]. According to this model the TP is initiated by electrons released from the cathode and proceeds by the Townsend ionization in initial electron avalanches.

The initial avalanches are produced between the cathode and some position distant from the cathode less

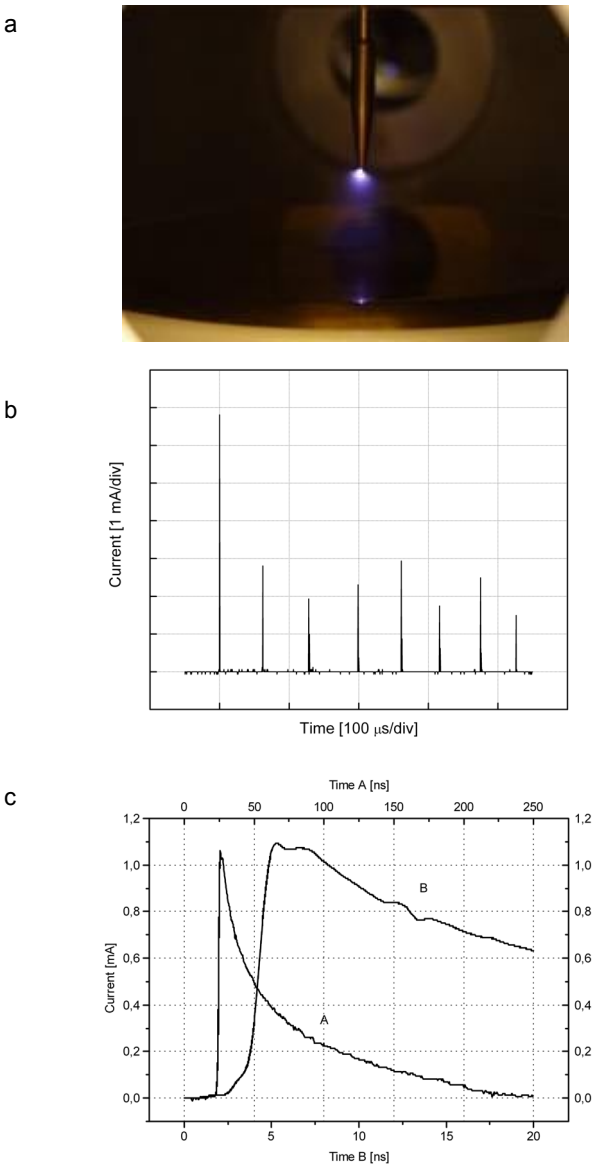

Fig. 1. **a) Negative corona discharge in a short point-to-plane gap, b) train of regular TPs measured in ambient air, c) leading edge of the regular TP in ambient air**

than 1 mm, where the ionization coefficient falls to zero. From the initial electron avalanches further generation of avalanches will result by secondary electron liberation at the cathode due to photoemission resulting in the fast TP current rise to the pulse maximum. Both Loeb and Alexandrov suggested that the TP current rise in ambient air cannot continue to values higher than 10^{-1} A because, in the time roughly equal to the short pulse rise time (see Fig. 1c), the electrons create a negative ion space charge through attachment to oxygen molecules at the perimeter (< 1 mm) of the ionizing zone. As a consequence, according to this theory, no free electrons can penetrate outside this narrow region. This is why it is generally accepted by the workers in the field of negative corona applications that the rest of the interelectrode space is filled solely with the negative ions.

However, the basic presumption of the Loeb-Alexandrov model on the current rise interruption due to the fast electron attachment is in sharp contrast to the fact that, when a step-wise voltage is applied to a negative corona gap in an electron nonattaching gas, the resulting glow corona formation is preceded by a peaked current signal of evidently the same mechanism as the fast TP rise and its initial decay in an electronegative gas, as O_2 and air[23–25]. Also, in the light of extensive results indication the mentioned independence of the TP rise time and magnitude on the cathode material[1–4], the fact that the Loeb-Alexandrov model, as well as the more recent computer simulation model by Morrow[26,27], are based on the presumption that the TP current rise is critically dependent on the cathode secondary emission, is a good reason to doubt about their validity.

In a contrast to the Loeb-Alexandrov model it has been suggested by several authors that the basic aspects of TPs formation can be explained on the basis of the streamer theory. According to this, the sequence of events leading to the TP formation can be envisaged as follows[2,25,28]:

At an initial stage of the development of a sequence of avalanches linked by the secondary emission from the cathode, the space charge created can shield itself from the external el. field, creating a streamer initiating plasma. If some "seed" electrons are presented just in front of the plasma, the avalanching in the locally enhanced field cause primary cathode- and anode-directed streamers to propagate. Thus, the feedback-to-cathode Townsend ionization mechanism fed by secondary electron emission from the cathode is supplanted by a faster feed-forward-to-gas streamer mechanism, where "secondary" electrons are created by photoionization in the gas. After an initial acceleration lasting for ~ 1 ns, velocity of the cathode-directed streamer increases exponentially to the order of 10^8 cm s^{-1} resulting in the TP rise due to the displacement current induced by the streamer movement in the cathode. The TP current rise is finished by the streamer arrival to the cathode and, subsequently, a low-current abnormal glow-discharge cathode spot is formed (Note that such process is theoretically analyzed in ref.[29]). The streamer-based model includes relevant physical factors that determine the development of Trichel pulses including the observed independence of the initial TP current peak on the electron detachment including and on the electron attachment and secondary electron emission (see refs.[23–25] and ref.[1–4], respectively). Contrary to the commonly held belief and in a sharp difference with the Loeb-Alexandrov model, the streamer-based model for TPs admits[2] the existence of a significant free electron current in negative corona discharges burning in ambient air even at distances from the cathode on the order of 1–10 mm. In fact, several indications for this can be found in refs.[14,30–32].

3. Conclusions

The above discussed and already experimentally well-verified streamer mechanism for TP formation strongly indicates the existence of free electrons in the drift region of negative corona discharges. Such free electrons, which can interact with the cold gas and induce reactions without back reactions in the drift region, may affect the chemical reaction in the corona gas volume as well as to induce surface reactions at the low-field anode.

This work was partly supported by the project R&D center for low-cost plasma and nanotechnology surface modifications CZ.1.05/2.1.00/03.0086 funded by the European Regional Development Fund and by the project 26240220042 supported by the Research & Development Operational Programme funded by the ERDF.

REFERENCES

1. Černák M., Hosokawa T.: Jpn. J. Appl. Phys. *27*, 1005 (1988).
2. Černák M., T. Hosokawa, S. Kobayashi, T. Kaneda: J. Appl. Phys. *83*, 5678 (1998).
3. Zahoranová A., Kúdelčík J., Paillol J., Černák M.: J. Phys. D: Appl. Phys. *35*, 762 (2002).
4. Zahoranová A., Šimor M., Černák M., Zahoran M., Kúdelčík J.: Czech. J. Phys. Suppl. D *52*, 886 (2002).
5. Eliasson B., Hirth M., Kogelschatz U.: J. Phys. D: Appl. Phys. *20*, 1421 (1987).
6. Abolmasov S. N., Kroely L., Roca P.: J. Phys. D: Appl. Phys. *41*, 165203 (2008).
7. Liu Ch., Marafee A., Hill B., Xu G., Mallinson R., Lobban L.: Ind. Eng. Chem. Res. *35*, 3295 (1996).
8. Kenkichi Nagato, Yasunori Matsui,Takahiro Miyata, Toshiyuki Yamauchi: Int. J. Mass Spectrom. *248*, 142 (2006).
9. Skalný J. D. et. al. : J. Phys. D: Appl. Phys. *37*, 1052 (2004).
10. Viner A. S., Lawless P. A., Ensor D. S., Sparks L. E.: IEEE Trans. Ind. Appl. *28*, 504 (1992).
11. Nashimoto K.: J. Imaging Sci. *32*, 205 (1988).
12. Pekarek S.: Eur. Phys. J. D *56*, 91 (2010).
13. Kurdel M., Morvová M.: Czech. J. Phys. *47*, 205 (1997).

14. Goldman M., Goldman A., Sigmond R. S.: Pure Appl. Chem. *57*, 1353 (1985).
15. Groza A. et. al. : Europhys. Lett. *68*, 652 (2004).
16. Napartovich A. P.: Proc. Int. Symp. on High Pressure Low Temperature Plasma Chemistry *1*, eds. H Wagner et al (Greifswald, Germany), 122, (2000).
17. Giacometti J. A.: IEEE Trans. Electr. Insul. *27*, 924 (1992).
18. Skalný J., M. Luknárová M., Dindošová D.: Czech. J. Phys. *38*, 329 (1988).
19. Goodman N., Hughes J. F.: J. Electrost. *60*, 69 (2004).
20. Machala Z., Tarabová B., Pelach M., Sipoldova Z., Hensel K., Janda M., Sikurova L.: Machala Z., Tarabová B., Pelach M., Sipoldova Z., Hensel K., Janda M., Sikurova L.: in Plasma for Bio-Decontamination, Medicine and Food Security, NATO Science for Piece and Security, Series A: Chemistry and Biology, 31 (2012)
21. Loeb L. B.: Electrical Coronas: Their Basic Physical Mechanism (Berkeley, CA: University of California) (1965).
22. Alexandrov G. N.: Sov. Phys. Tech. Phys. *8*, 161 (1963).
23. Černák M., Hosokawa T.: Appl. Phys. Lett. *52*, 185 (1988).
24. Černák M., Hosokawa T.: Jpn. J. Appl. Phys. *26*, L1721 (1987).
25. Černák M., Hosokawa T., Odrobina I.: J. Phys. D: Appl. Phys. *26*, 607 (1993).
26. Morrow R.: Phys. Rev. A *32*, 3821 (1985).
27. Morrow R.: Phys. Rev. A *32*, 1799 (1985).
28. Černák M., Hosokawa T.: Phys. Rev. A *43*, 1107 (1991).
29. Odrobina I., Černák M.: J. Appl. Phys. *783*, 635 (1995).
30. Černák M., Skalný J. D.: Czech. J. Phys. *34*, 926 (1984).
31. Leal Ferreira G. F., Oliviera O. N., Giacometti J. A.: J. Appl. Phys. *59*, 3045 (1986).
32. Gagarin A. G., Vigborchin V. Kh., Mitjuschin A. I.: Teplofiz. Vys. Temp. *4*, 823 (1983).

J. Halanda[a], A. Zahoranová[b], J. Kúdelčík[c], and Mirko Černák[a,c] *([a] Dep. of Experimental Physics, Comenius University, Bratislava, Slovak Republic; [b] Dep. of Physics, Faculty of Electrotechnical Engineering, University of Žilina, Žilina, Slovak Republic, [c] R&D Center for Low-Cost Plasma and Nanotechnology Surface Modifications, Faculty of Science, Masaryk University, Brno, Czech Republic):* **Chemical Aspects of Streamer Mechanism for Negative Corona Discharges**

It is explained that, contrary to the traditional Loeb-Alexandrov model for the negative corona current pulses formation, the more recent streamer-based model admits the existence of a significant free electron current in negative corona discharges burning in ambient air even at distances from the cathode on the order of 1–10 mm. The existence of such free electrons is in a sharp contrast to the commonly held belief that the low-field drift region of the discharge is filled solely with the negative ions. The importance of such free electrons for chemical reactions induced by negative corona discharges is discussed briefly.

CHEMICAL AND PHYSICAL EVALUATION OF HYDROPHOBIC pp-HMDSO LAYERS DEPOSITED BY PLASMA POLYMERIZATION AT ATMOSPHERIC PRESSURE

RICHARD KRUMPOLEC*[a], ANNA ZAHORANOVÁ[a], MIRKO ČERNÁK[a,b], DUŠAN KOVÁČIK[a,b]

[a] *Dep. of Experimental Physics, Faculty of Mathematics, Physics and Informatics, Comenius University, Mlynská dolina F2, 842 48 Bratislava, Slovak Republic,* [b] *R&D Center for Low-Cost Plasma and Nanotechnology Surface Modification, Faculty of Science, Masaryk University, Kotlářská 2, 611 37 Brno, Czech Republic*
krumpolec@fmph.uniba.sk

Keywords: plasma polymerization, hexamethyldisiloxane, glass, hydrophobic surface

1. Introduction

The deposition of various boundary layers is an important part of technology occurring in different areas. This considers great range of applications such as protective layers coatings, adhesion improvement, applications in Nano- & Bio- technology, and many other applications. The hydrophobic boundary layers deposition, e.g. by plasma polymerization could be one approach.

As "Plasma Polymerization", we consider the thin films deposition from mixture of monomers in plasma. It is possible to deposit various thin films with desirable physical and chemical characteristics using appropriate optimalization of operating parameters. Polymers formed by this technique, called as Plasma-Polymers, are generally highly branched and highly cross-linked due to radical fragmentation mechanism of polymerization. The resulting properties may be the high scratch resistance, insolubility as well as excellent adhesion to solid surfaces.

In this study we have worked with Hexamethyldisiloxane monomer (HMDSO $C_6H_{18}OSi_2$, $(CH_3)_3Si–O–Si–(CH_3)_3$). Therefore, the deposited plasma polymer was marked as pp-HMDSO. The chemical properties of obtained new polymer layers are presented.

2. Experimental setup

For plasma polymerization of hydrophobic polymer layers on the glass substrates a special reactor was constructed (Fig. 1). As the plasma source we used Diffuse Coplanar Surface Barrier Discharge[1,2] (DCSBD) fed by high voltage source (LIFETECH, s.r.o., Brno, Czech Republic).

In reactor chamber from plexiglass a movable cart which moved a sample above DCSBD plasma was placed.

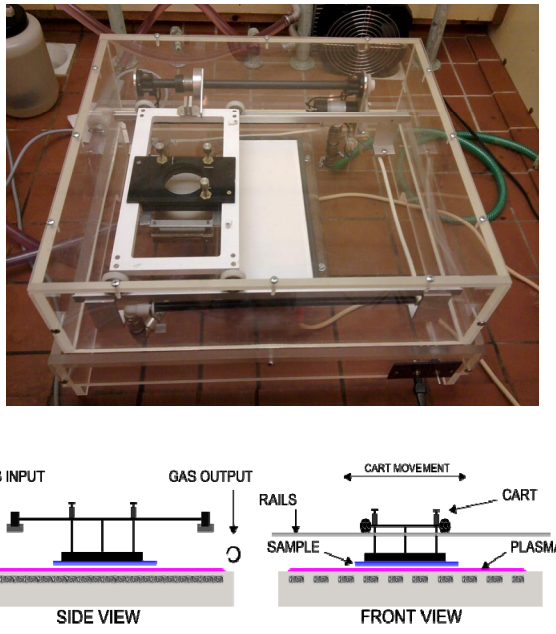

Fig. 1. **Reactor based on DCSBD for plasma polymerization**

The distance of sample's surface from ceramic surface of coplanar discharge could be adjusted as well as the velocity of the cart (Fig. 1).

As the glass samples for plasma polymerization the glass slides for optical microscopy with dimensions 25.85 × 75.9 × 1.0 mm were used. The as-received samples were inhomogeneous. To ensure the same surface properties of every glass sample they were cleaned before every experiment by this chemical cleaning procedure:

- 5 – minutes cleaning in acetone in ultrasonic bath,
- 5 – minutes cleaning in isopropyl-alcohol in ultrasonic bath,
- 5 – minutes cleaning in distilled water in ultrasonic bath.

After cleaning in ultrasound bath every sample was dried with nitrogen stream. For AFM, SIMS or XPS analyses we used smaller samples (the same material and cleaning procedure) with dimensions max. 10×10 mm.

The polymerization was carried out in dynamic mode for homogeneous plasma-polymerization treatment. The glass samples were polymerized 1 minute in N_2/HMDSO mixture vapour (concentration of HMDSO monomer admixture in nitrogen was set to $c = 0.147$ mmol l^{-1}). The input power to discharge was set up to 270 W. The distance of sample surface was set to 0.3 mm. After the entire layer deposition the samples were stored under ambient laboratory conditions. The deposited polymer layers were

hydrophobic with contact angles values of 90°–100° (measured for distilled water).

As the monomer for plasma polymerization a Hexamethyldisiloxane (HMDSO, as-received from Merck, Germany) with nitrogen (5.0) as a carrier gas were used.

A N_2/HMDSO mixture was carried out by system with two thermal mass flowmeters RED-Y (max. 10 l min^{-1} and 2 l min^{-1} respectively). The monomer temperature was controlled by thermocouple senzor.

3. Analytical methods

In order to investigate the morfology properties of deposited polymer layers SEM and AFM methods were used. SEM analysis was carried out by the Vega II SBH scanning electron microscope. The analyzed samples were non -conducting so they had to be coated with a thin Au-layer (~ 17–20 nm) with magnetron sputtering by BIO-RAD SEM Coating System (Microscience Division). The surface of plasma-polymer films was evaluated also by Atomic Force Microscopy (Solver P47-PRO).

The FTIR spectrum of polymer layers on glass substrates were recorded by BRUKER VECTOR 22 spectrometer using diamond Attenuated Total Reflection with Diamond/ZnSe polarization accessory from MIRacle™ (PIKE Technologies) The diamond was set at 45 degrees and other measurement settings were 20 scans, resolution 4 cm^{-1}, measuring range 4000–500 cm^{-1}.

The XPS spectrum used for component analysis of films was measured by Phoibos 100 XPS device from Specs company. The photoelectrons were detected by hemispheric analyzer in FAT regime. The photoelectron energy spectrum was calibrated according to energy of carbon bond C-C which characteristics energy is 284.5 eV. The spectra were analyzed and evaluated in CasaXPS software.

SIMS analysis was carried out on the TOF SIMS IV device (from ION-TOF Company, Münster, Germany). For ion bombardment of the sample's surface the bismuth ion gun producing Bi^+ ions (25 keV ion energy and current 1 pA) was used. The mass spectrum was analyzed in positively and negatively polarity on the total surface area of 100×100 μm^2. As the glass is dielectric, the electron gun for surface charge compensation was used.

4. Results

4.1. Morfology Analysis of Polymer Layers

The SEM analysis was performed on the samples stated as S1, S2, S3 which parameters are listed in the Table I. Sample S3 was treated after plasma polymerization by DCSBD plasma to study curing of deposited polymer film. The AFM operated in semicontact mode scanned the sample's surface on the scale of 100 μm^2. As the qualitative parameters for roughness rating (evaluation) R_q (RMS) and R_a (average roughness) were selected.

As the results show in Table II, the deposited polymer layers are smooth with $R_q < 1$ nm. The maximum roughness for every sample is under 10 nm except sample S3. We assume it is due to plasma post-treatment which caused increase of average roughness up to 19 nm.

Table I
List of analyzed samples and their treatment parameters

Sample	S1	S2	S3
Polymerization time, sec	60	30	60[a]
Input power, W	270	270	270
N_2/HMDSO mixture concentration, mmol l^{-1}	0.147	0.147	0.147

[a] The S3 sample was treated by N_2 plasma after plasma polymerization for 10 seconds to cure and stabilize the layer

Table II
Surface roughness of pp-HMDSO layers from Table I

Sample	R_q [nm]	R_a [nm]	Max. Roughness [nm]
S1	0.491	0.378	8.015
S2	0.679	0.543	7.159
S3	0.598	0.451	19.221
As-received glass	0.549	0.356	16.333

The SEM imaging revealed very smooth surface character even over maximum total area 700×700 μm^2 and all zooms from 300× to 100 000× in which the surface was scanned.

4.2. Chemical Analysis of Polymer Layers

FTIR analysis of polymer layer surfaces

FTIR spectrum of polymer layer on glass in the range 3600–1200 cm^{-1} can be seen in the Fig. 2. The broad wave number region of 3000–3600 cm^{-1} of infrared spectra is associated to valence vibrating states of primary (straight) amine functional groups of NH, NH_2 (ref.[3]). In the same region the peak associated with vibrating O-H and C-H states[4] was identified.

As we mentioned before, the monomer fragmentation goes on through radical mechanism[5]. The HMDSO molecule is broken to smaller units. Therefore on the layer surface we can identify the methyl CH_n groups, indicated by valence vibrational states of C-H in the band 2980–2850 cm^{-1} (ref.[6,7]).

Since used diamond ATR crystal technique we could not detect reliably the intensities in the range

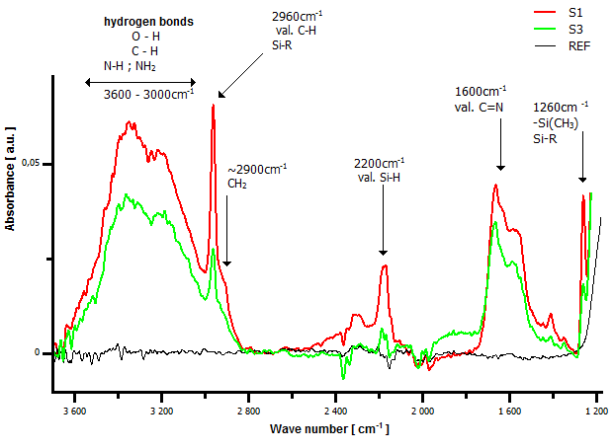

Fig. 2. **Selected FTIR spectrum of analyzed pp-HMDSO samples in the wavenumber range 3600–1200 cm^{-1}. REF = reference as-received glass sample**

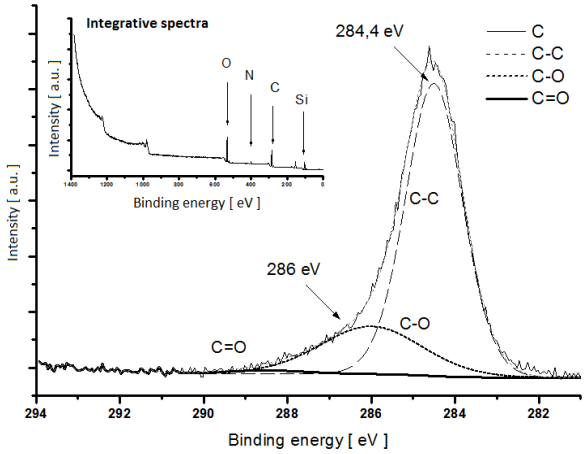

Fig. 3. **High-resolution XPS spectrum of C 1s for sample S1**

1950–2200 cm^{-1}, where e.g. typical C≡N bond at about 2200 cm^{-1} lies.

A significant increase of peak's amplitudes is also apparent in the range 950–1100 cm^{-1} from Si-O-Si bond and of the Si-H a Si-CH$_n$ states in the range 800–750 cm^{-1} respectively (Not shown in the Fig. 2).

XPS analysis of polymer layer surfaces

We interested in percentage proportion of elements creating the pp-HMDSO films on two samples S1 and S2 (with different time of polymerization). Namely the Si 2p, O 1s, C 1s a N 1s levels were studied as can be seen in the Fig. 3. In Fig. 4, the values of percentage proportion for sample S1 are compared to the XPS analysis of pure glass without hydrophobic treatment. The element composition for sample S2 with half polymerization time was quite the same as for sample marked as S1.

SIMS analysis of polymer layer surfaces

As expected, in the SIMS mass spectrum the most significant peaks came from CH$_x$ methyl groups bonded to SiO and SiO$_2$ groups respectively. The proportional distribution as $I_C < I_{CH} < I_{CH2} < I_{CH3}$ we observed in the mass spectrum of every sample. The I_x is intensity associated to the peak of X element. The intensities were calculated as the Corrected Area.

In addition to methyl groups bonded to Si or SiO we detected also amine (e.g. C$_x$H$_y$NO, SiCH$_x$N$_y$) and OH groups bonded to SiO$_2$, SiO or Si. The organic character of deposited films is confirmed also by organic functional groups as well as C_H, C_{H2}, C_{H3}, and more difficult C$_x$H$_y$ fragments respectively. The intensity of Si$^+$ ion decreases in sequence from sample S3 to sample S1. In case of sample S2 this is causes by higher organic C$_x$H$_y$ groups bonded from monomer due to longer polymerization time while decreasing of Si$^+$ ion detected on sample S1. As the

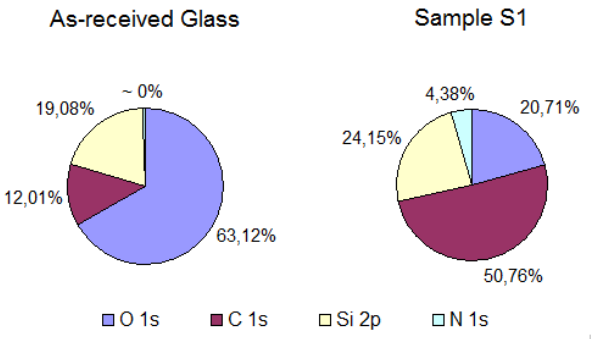

Fig. 4. **Percentage proportion of oxygen, carbon, silicon and nitrogen for sample S1 compared with as-received glass sample**

direct result of plasma post-treatment of pp-HMDSO film the organic C$_x$H$_y$ groups are wiped off (Fig. 5), because of lower energy bonds compared to the silicon and oxygen atoms. And further, it results in highest peak Si$^+$ ion for sample S3 compared to samples S1 and S2.

In the SIMS mass spectrum it was evidently visible the fragmentation series of $Si-O_x-C_n-H_{3n}-\{CH_3\}_n$ and $Si-O_x-C_n-H_{3n}-\{CH_2\}_n$ respectively.

The mechanical properties of pp-HMDSO layers were evaluated by Fischerscope H100 nanoindentor. The S1 sample was approximately 150 nm thick, while microhardness was 7 GPa, with elastic module of 70 GPa.

The stability of hydrophobic coatings was monitored of 120 hours after plasma polymerization and any "Ageing Effect" was observed. The average contact angle remained constant with significant decrease of value dispersion. Moreover the coated samples pass through the 120 minutes boiling test in distilled water.

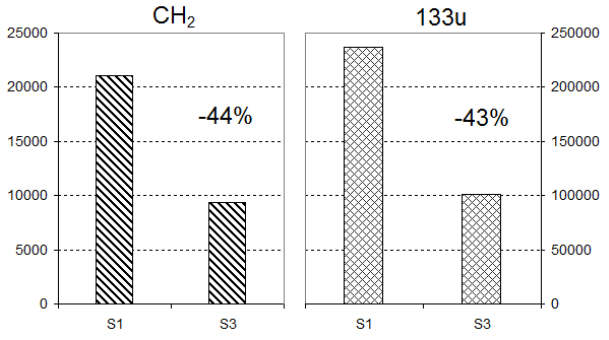

Fig. 5. **Removal of organic C_xH_y groups by plasma post-treatment. Decrease of intensity for CH_2 and heavier 133u with $(CH_2)_n$ organic groups peak fragment without and after plasma post-treatment (S1 vs. S3 samples). The symbol "u" refers Atomic Unit Mass**

5. Discussion

Trunec et al.[7] used for thin layer deposition of polymer pp-HMDSO layers on glass substrates nitrogen plasma generated by APGD discharge. Depending on the monomer concentration they observed the filamentary discharge or homogeneous plasma respectively. In the case of samples deposited in filamentary DBD they observed the sharp peaks with average height of up to 150 nm. In homogeneous regime of plasma generation they deposited the layers with average roughness of 7.9 nm, at deposition time 10 minutes.

According to the XPS analysis of our pp-HMDSO layers we conclude the percentage composition of carbon, oxygen, silicon and nitrogen is
n [%] (C : O : Si : N) = ~ 50 : 21 : 24 : 5.

For comparison, the authors in ref.[7] obtained this elements rate approximately in the ratio 41 : 26 : 15 : 17.

In the hexamethyldisiloxane molecule, the carbon to silicon atoms ratio is equal to 3. Based on the results of our XPS measurements of films we conclude this ratio decrease for the pp-HMDSO to value of 2. This change could be a consequence of the cross-linking during plasma polymerization process of the HMDSO molecule.[8]

As a result of plasma polymerization, the deposited pp-HMDSO films were characterized by high cross-linking with quite complex chemical structure. The most significant changes in FTIR absorbance spectrum of samples (compared to the pure glass) we observed at wave numbers 800–750 cm^{-1} (assigned to Si-O-Si; $Si-CH_n$), 1100–950 cm^{-1} (Si-O-Si; O-Si-O), 1260 cm^{-1} ($Si-CH_n$). Similarly, the highest IR intensity changes were observed at ~ 2960 cm^{-1} (assigned to valence vibration states of C-H, $Si-CH_n$) and around wave numbers of 2200 cm^{-1} (valence Si-H).

These observations are in good agreement with Szalowski´s et al. paper[9], where polymer coatings on glass in nitrogen plasma at atmospheric pressure were deposited too. In addition, the authors deposited polymer layers in the presence of substrate heating (~ 400 °C) and the total deposition time was 15 minutes.

Paulussen et al.[8] deposited the polymer layers on polished SiO_2 surface of silicon (deposition time 2 minutes) in nitrogen plasma generated by barrier discharge. They present the chemical composition of pp-HMDSO layers from XPS analysis as follows:
n [%] (C : O : Si : N) = ~ 50 : 24 : 24 : 2. As you can notice, it is similar rate as in our case presented earlier. Moreover, in the FTIR spectra were observed not only vibrations of $Si-(CH_3)_n$; $(CH_3)-Si-O-Si-(CH_3)$; C-O, but also from hydrogen – carbon and hydrogen – oxygen bonds C-H and O-H.

6. Conclusion

The possibilities to employ the plasma generated by DCSBD discharge for atmospheric pressure plasma polymerization of HMDSO monomer in nitrogen carrier gas were studied. The process of plasma polymerization is quite a complex, with a plenty of free parameters. The stable hydrophobic pp-HMDSO thin layers on the glass substrates were coated.

The polymer character of the coated layers was confirmed by the means of XPS, SIMS and FTIR analyses. After the XPS analysis the detail percentage of carbon, oxygen, silicon and nitrogen was obtained as n [%] (C : O : Si : N) = ~ 50 : 21 : 24 : 5. The AFM analysis, as well as SEM imaging, confirmed the smooth surfaces of polymer layers. The roughness of pure glass substrates is in the order of ~ 20 nm. Therefore the cleaned, high quality samples (not only glass) is important necessity for deposition at atmospheric pressure. This could be important for technology view of thin layer deposition. One negative and undesirable effect was observed during plasma polymerization – the direct deposition of pp-HMDSO polymer layer on the dielectric surface of coplanar discharge. The layer creates the additional dielectric barrier which implies the change of ignition voltage. On the other hand we have not observed any change in electrical characteristic of the discharge for HMDSO admixture of nitrogen working gas.

The DCSBD was successfully studied for plasma surface treatment, activation or cleaning of various types of materials[1,2]. In this study the hydrophobic coatings on glass substrates by plasma assisted polymerization were deposited. Our results show the possibility to employ DCSBD plasma for plasma assisted layer deposition. But we also see same drawback which should be solved in the future as we mentioned before. Apart from many advantages, the plasma polymerization approach also suffers from the serious disadvantage of high monomer and carrier gas consumption which are not efficient enough.

The authors express their thanks to M. Zahoran who performed SEM measurements and T. Plecenik for AFM analyses.

This work is the result of the project implementation: 26240220002 and 2622020004 supported by the Research & Development Operational Programme funded by the ERDF. Also, this research was partially supported by Comenius University in Bratislava under Grant UK No. UK/456/2012.

This research has been supported by the project R&D center for low-cost plasma and nanotechnology surface modifications CZ.1.05/2.1.00/03.0086 funding by European Regional Development Fund.

REFERENCES

1. Černák M. et al.: Eur. Phys. J. Appl. Phys. *47*, 22806 (2009).
2. Černák M. et al.: Plasma Phys. Control. Fusion *53*, 124031 (2011).
3. Milata V. et al.: *Applied Molecular Spectroscopy* – in slovak. STU in Bratislava, Bratislava 2008.
4. Gonzales-B. J. et al.: J. Appl. Polym. Sci. *62*, 375 (1996).
5. Fridman A.: *Plasma Chemistry*. Cambridge University Press, New York 2008.
6. Li K., Gabriel O., Meichsner J.: J. Phys. D: Appl. Phys. *37*, 588 (2004).
7. Trunec D. et al.: J. Phys. D: Appl. Phys. *37*, 2112 (2004).
8. Paulussen S., Goosens O., Vangeneugden D.: *International Symposium on Plasma Chemistry*: Abstracts and Full-Papers CD. *Taormina, Italy, June, 22-27, 2003* (R d'Agostino et al., ed.), Taormina, Italy 2003.
9. Szalowski-Sch K. et al.: Plasmas Polym. *5*, 173 (2000).

R. Krumpolec[a], A. Zahoranová[a], M. Černák[a,b], and D. Kováčik[a,b] *([a] Dep. of Experimental Physics, Faculty of Mathematics, Physics and Informatics, Comenius University, Bratislava, Slovak Republic; [b] R&D Center for Low-Cost Plasma and Nanotechnology Surface Modification, Faculty of Science, Masaryk University, Brno, Czech Republic):* **Chemical and Physical Evaluation of Hydrophobic pp-HMDSO Layers Deposited by Plasma Polymerization at Atmospheric Pressure**

This work deals with plasma polymerization deposition of hydrophobic layers onto glass substrates at atmospheric pressure. The hexamethyldisiloxane (HMDSO) organosilicon monomer was used as precursor for plasma polymerization in nitrogen working gas. The so-called Diffuse Coplanar Surface Barrier Discharge was used as a source of non-equilibrium non-thermal plasma. The pp-HMDSO thin films were studied by the means of SEM, AFM, FTIR, XPS and SIMS measurements. Our research revealed that smooth, polymer-like, hydrophobic and transparent in visible range thin films were deposited on the glass substrates. The results indicate that DCSBD discharge can be used for thin films deposition by the means of plasma polymerization process at atmospheric pressure.

THE EFFECT OF SURFACE CLEANING AND REMOVING OF ORGANIC CONTAMINANTS FROM SILICON SUBSTRATES AND ITO GLASS BY ATMOSPHERIC PRESSURE NON-THERMAL PLASMA

VERONIKA MEDVECKÁ*[a], ANNA ZAHORANOVÁ[a], DUŠAN KOVÁČIK[a,b], JÁN GREGUŠ[a]

[a] *Dep. of Experimental Physics, Faculty of Mathematics, Physics and Informatics, Comenius University, Mlynská dolina F2, 842 48 Bratislava, Slovak Republic,* [b] *R&D Center for Low-Cost Plasma and Nanotechnology Surface Modifications, Faculty of Science, Masaryk University, Kotlářská 2, 611 37 Brno, Czech Republic*
Veronika.Medvecka@fmph.uniba.sk

Keywords: DCSBD, silicon substrates, ITO glass, cleaning, organic contaminants

1. Introduction

Silicon is the most used material in semiconductor industry and photovoltaics. In the form of wafers, silicon serves as the basis for integrated circuits and multilayer technologies – Micro-Electro-Mechanical Systems (MEMS) or Silicon on Insulator (SOI). Semiconductor industry is affected by the miniaturization and what is accentuated is the purity, flatness and smoothness of substrate surface.

Indium tin oxide (ITO) is the solid solution of indium oxide (In_2O_3) and tin oxide (SnO_2) and it is heavily-doped n-type semiconductor. Due to high electrical conductivity and optical transparency in visible spectra, it is one of the most used transparent conductive oxides (TCO) as coating for many optical application – flat displays, organic or polymer light-emmiting diodes (OLED, PLED), IR-reflecting or Joule heating coating, gas sensors, etc.

In photovoltaics, 90 % of solar cells are produced from silicon[1]. Besides silicon and other semiconductors, solar cells are prepared from another materials able to generate electric charge by the light impact – thin films solar cells with organic light-absorbing dyes (DSSC), organic polymer materials[2,3] and semiconductors[4], etc. For improving of efficiency, new technologies are also used – multijunction, tandem, or quantum dot cells. Electrodes in the mentioned systems are often composed of TCO, mainly ITO thin film.

The preparation of semiconductor devices contains hundreds of steps and 10–15 % of them include cleaning and activation of surface. At present, the most used techniques are wet chemical cleaning methods. The standard model for cleaning of semiconductors was suggested and developed by Werner Kern in 1960. It is called RCA (ref.[5]), which is a type of wet chemical method using aggresive chemicals, which are toxic, environmentally unsuitable and non-biodegradable. At present, more economic and environmental alternative processes are investigated.

Many procedures in semiconductor industry are replaced by plasma. For cleaning of semiconductors low pressure plasma has been already used, but the necessity of vacuum equipment extends treatment time and enhances cost of method.

For this study a unique type of dielectric barrier discharge – Diffuse Coplanar Surface Barrier Discharge (DCSBD)[6] was used for removal of the organic contamination (2-propanol) from three types of silicon substrates. Moreover, comparative study of cleaning effectiveness of 2-propanol and DCSBD on the ITO glass samples was carried out. DCSBD produces non-thermal diffuse plasma in ambient air at atmosperic pressure. This type of plasma source was succesfully used for plasma treatment of nonwoven[7,8] , aluminium[9], wood[10], glass[11], or ozone production[12].

2. Experimental setup and samples

DCSBD consists of many parallel silver electrodes embedded in Al_2O_3 ceramics. DCSBD is powered by sinusoidal voltage with amplitude 15 kV (peak-to-peak) and frequency 16–18 kHz. More technical details are described in work of M. Šimor[13].

Experimental arrangement (Fig. 1) consist of static DCSBD discharge (Fig. 1-1) and moveable sample holder (Fig. 1-2) with possibility of treatment time adjusting in plasma in dynamic regime.

Silicon (111), N-type doped with phosphorus (ON Semiconductors, Czech Republic) with resistivity (33–45)·10^{-3} Ω m was used as a substrate. The diameter of the wafer was 100.0±0.5 mm and its thickness was 381±25 μm. Three types of silicon surfaces were prepared as follows:

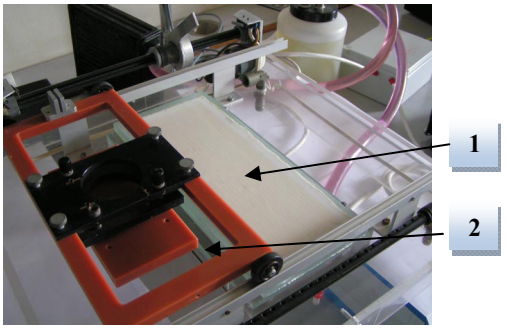

Fig. 1. **Experimental arrangement with main parts:** 1 – DCSBD, 2 – movable sample holder

a) "as received" silicon precleaned with acetone, 2-propanol and distilled water for 6 min in each liquid using sonication,
b) silicon pre-cleaned as in A), then thermally oxidized in O_2 atmosphere at 600 °C for 1 h
c) silicon pre-cleaned as in A), then rinsed in aqueous solution of hydrofluoric acid (HF/H_2O: 1/10 in volume).

Sample A was covered with a thin layer of native oxide. Thermal oxidation of sample B caused dehydration (removing of OH-groups) and increasing of oxide layer thickness. Immersion in HF dilution in sample C etches native oxide and creates hydrophobic H-terminated surface.

ITO glass samples (Präzisions Glas & Optik, GmbH, Germany) of CEC 015S type with ITO coating thickness of 120 nm were prepared on selected white float glass with thickness 1±0.1 mm and surface resistivity ≤ 15 Ω/□ (typical value 12,5 Ω/□).

3. Results and discussion

Isopopyl alcohol (IPA, 2-propanol, $(CH_3)_2CHOH$) was used for reproducable contamination of silicon samples. This chemical is often applied as a cleaning agent in electronics because of good dissolution of wide range non-polar compounds. IPA is also used as a solvent in other industrial processes, in medical application for disinfection, as fuel additives, etc.

The silicon samples marked A, B and C were rinsed in ultrasonic IPA bath for 3 min. In order to study the effect of the plasma treatment on the contamination removal, the samples were treated with DCSBD plasma in 0.3 mm distance from the Al_2O_3 ceramics. The input power was 300 W and the exposure time was 10 s. The parameters for plasma treatment were chosen according to previous research[14].

Attenuated Total Reflectance Fourier Transform Infrared Spectroscopy (ATR-FTIR) was performed with Bruker Vector 22 FT-IR spectrometer, equipped with additional Pike MIRacle™ accessories, working in the range from 4000 to 400 cm^{-1}. 20 scans were carried out with resolution of 4 cm^{-1}.

Si-O bond has weak ionic character[15] and it may exhibit very strong absorption in IR region. Relevant peaks and adequate bonds on silicon substrates are particularly Si-H bond and siloxanes. On each sample (A, B, C) peaks attributed to antisymmetric vibrations ν_{as}(Si-O-Si) (1105 cm^{-1}), valence vibrations Si-O-H (3700–3200 cm^{-1}) and H_2O bending in region from 1800 to 1400 cm^{-1} (ref.[16]) were observed. The peak at 611 cm^{-1} was identified as Si-Si bond[17]. On sample B – thermally oxidized silicon, it was possible to observe the characteristic peak (1240 cm^{-1}) of thermal oxide (Fig. 3) and with higher temperature of annealing its shift towards higher wavenumbers[13]. Si-H bonds[18], expected on H-terminated silicon (sample C) occure in region from 2280 to 2050 cm^{-1}. There was observed an area of IR absorption caused by CO_2 from air.

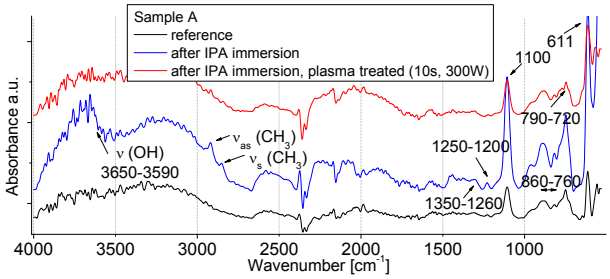

Fig. 2. **FTIR spectra of precleaned silicon (Sample A)**

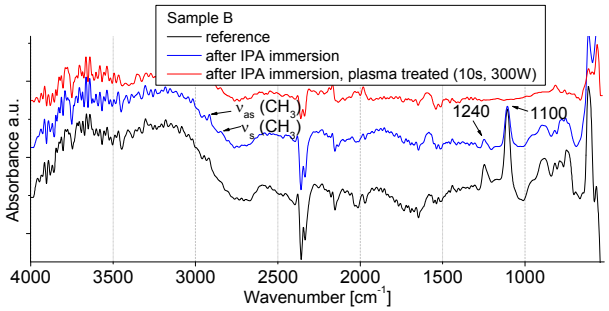

Fig. 3. **FTIR spectra of thermally oxidized silicon (Sample B)**

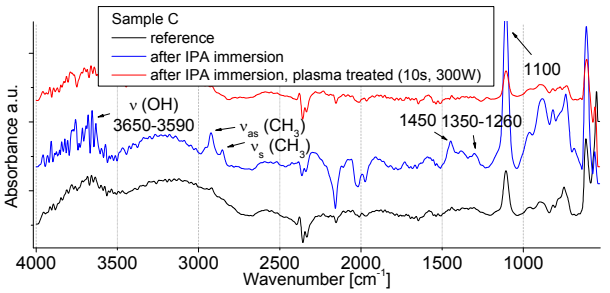

Fig. 4. **FTIR spectra of H-terminated silicon (Sample C)**

Changes after IPA immersion and plasma treatment were compared with IR spectra from the NIST database[19]. For alcohols and phenols, there are characteristic OH vibrations (3650–3590 cm^{-1}), for secondary alcohols such as the 2-propanol are specific deformation vibrations C-OH in region of 1350–1260 cm^{-1}. For H-bonds there is a shift to 1500–1300 cm^{-1} (ref.[20]). We can observe peak attributed to valence vibration C-O (1100 cm^{-1}) (ref.[20]) mainly in case of sample A (Fig. 2) and C (Fig. 4). It can overlap with the peak attributed to antisymmetric valence vibration of Si-O-Si – 1105 cm^{-1}. Organic contaminants on silicon are visible in region 600–1300 cm^{-1} (ref.[18]). In region 860–760 cm^{-1} there may exist valence vibrations Si-C (ref.[20]).

In case of sample C (Fig. 4) the peak at 1450 cm^{-1} was found. This peak was probably attributed to scissoring

deformation of CH_2 or antisymmetric deformation CH_3 (ref.[18]). Peaks of symmetric and antisymmetric valence vibrations of CH_3 (ref.[18,20]) was observable on each sample immersed in IPA. Intensity of peaks indicating IPA increased after IPA immersion and decreased after plasma treatment, mainly on samples A (pre-cleaned silicon) and C (H-terminanted silicon). Thermally oxidized silicon (Fig. 3) was relatively resistant to IPA contamination. The peaks were small after IPA ultrasonic bath and they decreased only slightly after plasma treatment. Moreover, peak observed at 1240 cm^{-1} (characteristic for thermally oxidized silicon) became extinct after plasma cleaning.

XPS signals were recorded using a Thermo Scientific K-Alpha XPS system equipped with a micro-focused, monochromatic Al Kα X-ray source (1486.6 eV). Measurement was carried out in argon (partial pressure $2 \cdot 10^{-7}$ mbar). The *Avantage* 4.75 software was used for digital acquisition and data processing. Spectral calibration was determined by using the automated calibration routine and the internal Au, Ag and Cu standards supplied with the K-Alpha system.

XPS measurements revealed increase of carbon compounds after IPA immersion and their decrease after plasma treatment. The effect of plasma treatment was compared on samples with and without IPA precleaning (Tab. I). The influence of plasma treatment was significant mainly in case of pre-cleaned (A) and H-terminated (C) silicon samples. During the preparation of thermal oxide (B) the organic contaminants are removed because of high temperature, therefore the thermally oxidized silicon is relatively resistant to IPA contamination. Fig. 5–7 show relative quantities of C-bonds obtained from deconvolution of C1s peak. The composition of bonds before and after plasma treatment indicated, that plasma is suitable for removal of IPA residues as well as for removal of other organic contamination mainly from samples A and C.

Table I
Chemical composition of silicon samples: IPA removing with plasma treatment (300 W, 10 s) measured with XPS

		Atomic concentration [%]			
		O1s	Si2p	C1s	N1s
Si precleaned (Sample A)	Reference	30	59	5	
	Ref + plasma	39	52	4	
	IPA	29	55	16	
	IPA + plasma	42	52	5	1
Si thermally oxidized (Sample B)	Reference	62	36	2	
	Ref + plasma	59	37	4	
	IPA	48	47	5	
	IPA + plasma	51	45	4	
Si H-terminated (Sample C)	Reference	10	70	11	9
	Ref + plasma	44	47	4	1
	IPA	56	23	20	1
	IPA + plasma	40	52	6	1

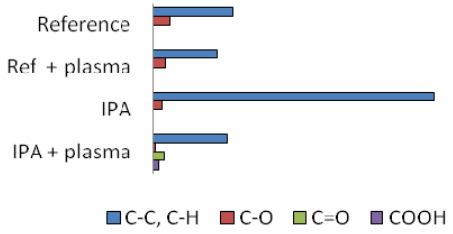

Fig. 5. **Relative quantities of C-bonds on precleaned silicon (A)**

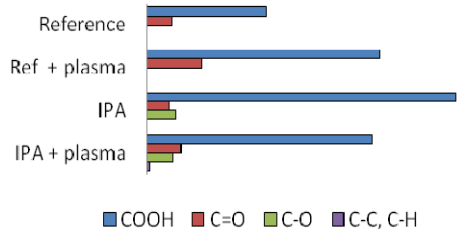

Fig. 6. **Relative quantities of C-bonds on thermally oxidized silicon (B)**

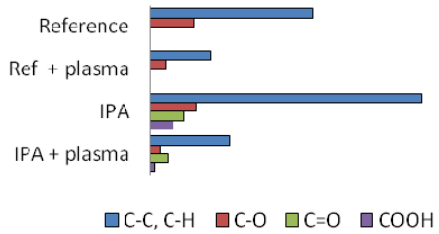

Fig. 7. **Relative quantities of C-bonds on H-terminated silicon (C)**

In this study we also compared cleaning effectiveness of IPA and plasma on ITO glass by XPS measurements. ITO glass was immersed in IPA for 5 min in ultrasonic bath and then was treated with plasma (300 W, 5 sec). Parameters for the plasma treatment of ITO glass were chosen with reference to previous research[21]. The sample without wet cleaning (reference sample) was studied also before and after plasma treatment. In Tab. II, it is shown that the content of carbon compounds decreased after IPA immersion and the oxygen content increased (due to increase of indium and tin oxides). In case of the reference sample without precleaning IPA caused partial removing of organic contaminants. The higher decrease of carbon compounds after plasma treatment of reference and IPA cleaned samples indicates that plasma removes organic contaminants as well as IPA residues. The relative quantities of C-bonds obtained from deconvolution of C1s peak are shown in Fig. 8. IPA removed contaminants with simple C-C, C-O bonds only partially. Plasma treatment caused better removal of both, contaminants with simple

Table II
Chemical composition of ITO glass-IPA removing with plasma treatment (300 W, 5s) measured with XPS

	Atomic concentration[%]			
	C 1s	In 3d	O 1s	Sn 3d
Reference	51	15	32	2
Ref + plasma	11	28	58	3
IPA	31	25	41	3
IPA + plasma	11	29	57	3

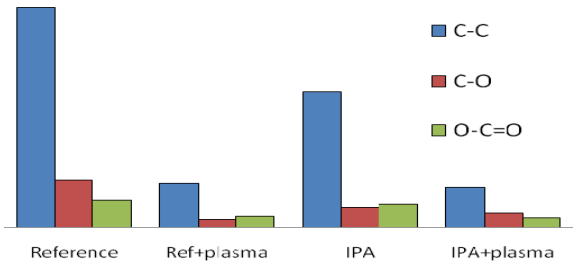

Fig. 8. **Relative quantity of C-bonds on ITO glass**

bonds and contaminations with more complicated bonds as O-C=O.

4. Conclusion

FTIR spectroscopy investigation of three type of silicon surfaces shows characteristic peaks indicating 2-propanol after IPA immersion and removing of IPA after plasma treatment using DCSBD. Only the thermally oxidized silicon was relatively resistant to 2-propanol.

Changes in chemical composition of surface measured by XPS approve increase of carbon compounds after IPA immersion and decline after plasma treatment, mainly on precleaned silicon and silicon rinsed in hydrofluoric acid. For comparison of cleaning effectiveness XPS measurement of ITO glass reference (as received) and IPA cleaned samples before and after plasma treatment was made. Changes in chemical composition indicate that plasma generated by DCSBD is suitable for organic contaminants removing and more effective than 2-propanol, which is often used for cleaning in electronics, semiconductor industry, medicine, etc.

This research has been supported by the project R&D center for low-cost plasma and nanotechnology surface modifications CZ.1.05/2.1.00/03.0086 funded by European Regional Development Fund., by the projects: 26240220002 and 2622020004 supported by the Research & Development Operational Programme funded by the ERDF and by UK grant UK/434/2012.

REFERENCES

1. Müller A., Ghosh M., Sonnenschein R., Woditsch P.: Mat. Sci. Eng., B *134*, 257 (2006).
2. Zunger A., Wagner S., Petroff P.M.: J. El. Mat. *22*, 3 (1993).
3. Chevaleevski O., Larina L.: Korean J. Chem. Eng. *18*, 403 (2001).
4. Brabec Ch. J.: Solar Energy Materials & Solar Cells *83*, 273 (2004).
5. Kern W.: J. Electrochem. Soc. *137*, 1887 (1990).
6. Černák M.: Patent WO 2007/142612 A1 2007, (2007).
7. Černák M., Černáková Ľ., Hudec I., Kováčik D., Zahoranová A.: Eur. Phys. J. – Appl. Phys. *42*, 22806 (2009).
8. Černáková Ľ., Szabová R., Wolfová M., Buček A., Černák M.: Fibres & Textiles in Eastern Europe *15*, 121 (2007).
9. Bónová L., Buček A., Plecenik T., Zahoranová A., Černák M.: Chem. Listy *102*, s1452 (2008).
10. Ondrášková M., Ráheľ J., Zahoranová A., Tiňo R., Černák M.: Plasma Chem. Plasma Proc. *28*, 203 (2008).
11. Buček A., Homola T., Aranyosiová M., Velič D., Plecenik T., Havel J., Sťaheľ P., Zahoranová A.: Chem. Listy *102*, s1459 (2008).
12. Šimek M., Homola T.: *28th ICPIG, Prague, Czech Republic, July 15-20, 2007* (Poster no. 3P10-29).
13. Šimor M., Ráheľ J., Vojtek P., Černák M., Brablec A.: App. Phys. Lett. *81*, 2716 (2002).
14. Zahoranová A., Medvecká V., Kováčik D., Plecenik T., Greguš J., Černák M.: *HAKONE XII, Trenčianske Teplice, Slovakia, 12.-17.9.2010,* Book of Contributed Papers (Országh, J., Papp, P., Matejčík, Š., ed.) p. 521.
15. Pauling L.: Am. Mineralogist *65*, 321(1980).
16. Amirfeitz P., Bengtsson S., Bergh M., Zanghellini E., Borjesson L.: J. Electrochem. Soc. *147*, 2693 (2000).
17. Vásquez-A. M. A., Águila Rodríguez G., García-Salgado G., Romero-Paredes G., Pena-Sierra R.: Revista Mexicana De Fi´sica *53*, 431 (2007).
18. Mayo D. W., Miller F.A., Hannah R. W.: *Course Notes on The Interpretation of Infrared and Raman Spectra.* J. Wiley, New Jersey 2003.
19. WebBook Chemie, NIST, [online] http://webbook.nist.gov/cgi/cbook.cgi?ID=C67630&Units=SI&Type=IR-SPEC&Index=3#IR-SPEC(4.5.2012).
20. Milata V., Segľa P., Brezová V., Gatial A., Kováčik V., Miglierini M., Stankovský Š., Šíma J.: *Aplikovaná molekulová spektroskopia,* Slovenská technická univerzita, Bratislava 2008.
21. Homola T., Matoušek J., Medvecká V., Zahoranová A., Kormunda M., Kováčik D., Černák M.: Appl.Surf. Sci. *258*, 7135 (2012).

V. Medvecká[a], A. Zahoranová[a], D. Kováčik[a,b], and J. Greguš[a] *([a] Dep. of Experimental Physics, Comenius University, Bratislava, Slovak Republic; [b] R&D Center for Low-Cost Plasma and Nanotechnology Surface Modifications, Faculty of Science, Masaryk University, Brno, Czech Republic):* **Effect of Surface Cleaning and Removing of Organic Contaminants from Silicon Substrates and ITO Glass by Atmospheric Pressure Non-thermal Plasma**

Plasma generated by DCSBD was investigated for cleaning and removing of organic contaminants from semiconductor materials. ITO glass used in photovoltaics and three types of most often used silicon surfaces in semiconductor industry – precleaned silicon, thermally oxidized silicon and H-terminated silicon was studied. The changes in chemical bonds on silicon surfaces were investigated by FTIR. Removing of IPA from silicon substrates was observed by XPS measurements. Effectivity of DCSBD as cleaning agent in comparison with isopropylacohol was investigated on ITO glass samples by XPS measurement.

MULTIFUNCTIONAL TRANSPARENT PROTECTIVE COATINGS ON POLYCARBONATES PREPARED USING PECVD

VALENTIN MOCANU[a]*, ADRIAN STOICA[a,b], LUKÁŠ KELAR[a], DANIEL FRANTA[a,b], VILMA BURŠÍKOVÁ[a,b], ROMANA MIKŠOVÁ[c], VRATISLAV PEŘINA[c]

[a] *Dept. of Physical Electronics, Masaryk University, Kotlářská 2, 611 37 Brno,* [b] *CEITEC, Central European Instituteof Technology, Masaryk University, Brno,* [c] *Nuclear Physics Institute, Academy of Sciences of the Czech Republic, 250 68 Rež near Prague, Czech Republic*
vallym@mail.muni.cz

Key words: multilayered coatings, protective, transparent, polycarbonate

1. Introduction

The advantageous properties (light weight, unique mechanical, thermal and electrical behaviour and high freedom of design) of plastics favoured the replacing of glass in a wide range of industries. The thermoplastic material can be manufactured by injection moulding to complex formed transparent elements. Optical characteristics of polycarbonate are a comparatively high refractive index of about 1.58 (500 nm) and a high dispersion (low Abbe number)[1]. The disadvantages of this material are high birefringence, low mechanical hardness, and sensitivity to UV radiation. Because of the known disadvantages of plastics compared to glass, such the softer surface and sensitivity to weathering, there is a high demand for development of protective coatings against degradation upon exposure to environment ultraviolet light. Various efforts are under way to develop scratch-resistant coatings based on silica and siloxanes by applying sol-gel or plasma -enhanced chemical vapor deposition (PECVD) processes[2–4]. The degradation of polycarbonate by global UV radiation has been well studied because polycarbonates are prone to yellowing[5–7].

When ultraviolet attack occurs the material may have a color shift, become chalky on the surface, and/or crack. There are a number of methods to reduce this problem. The addition of carbon black to the polymer will usually absorb most UV radiation. Chemical inhibitors are available for certain plastics, which improve the UV resistance. Paint and silicone coatings can also be used to completely cover exposed surfaces to sunlight (UV radiation). To remedy these limitations, various methods of producing hard transparent protective coatings are applied[8]. Existing wet chemical coating technologies consist of several steps, e.g. curing by UV radiation or oven drying. Among various techniques, plasma is a complex source of energy for surface modification, due to the large variety of components, such as excited and ionised particles, photons, radicals, with all of these species being capable of inducing chemical reactions, both in the plasma volume and at its interface with solid surfaces. There are two ways to plasma modify the surface properties of polymers, either by introducing new functional groups by surface grafting using noncoating plasmas, or by deposition of organic or inorganic films with the desired properties using coating plasmas[9].

We used the plasma-enhanced chemical vapour deposition method based on hexamethyldisiloxane (HMDSO) monomer and oxygen mixture to deposit protective films on polycarbonate surface.

Table I
Deposition parameters for the selected samples: n is the flow rate ratio $n= Q_{HMDSO}/(Q_{HMDSO} +Q_{O2})$, where Q_{O2} is the oxygen flow rate, Q_{HMDSO} is the monomer (HMDSO, $Si_2OC_6H_{18}$) flow rate, P is the applied power, U_b is the self bias voltage on the bottom substrate holder electrode, p is the average pressure, the relative error of the listed parameters is around 3%

No	Q_{O2} [sccm]	n	P [W]	U_b [V]	p [Pa]
VI01	5.2	0.66	50	–140	23.4
VI02	2.9	0.80	50	–175	14.5
VI03	5.2	0.66	50	–160	24.5
VI05	9.8	0.47	100	–185	36.4
VI06	20	0.31	100	–180	60.0
VI07	50	0.15	100	–111	111
VI09	4.9	0.64	100	–278	23.3
VI10	9.7	0.48	100	–216	39.0
VI11	9.7	0.47	50	–119	39.0
VI12	4.9	0.66	50	–196	23.0
VI13	4.7	0.66	75	–200	24.0
VI14	2.9	0.71	50	–240	15.0
VI15	4.9	0.52	50	–160	23.0
VI16	6.6	0.50	50	–150	31.0
VI17	9.7	0.52	50	–111	38.9
VI18	9.7	0.52	50	–107	38.0
VI19	7.0	0.60	50	–105	33.5
VI20	5.0	0.50	50	–192	24.8

2. Experimental

The films were prepared in low pressure r.f. glow discharges burning in mixtures of hexamethyldisiloxane (HMDSO, $Si_2OC_6H_{18}$) monomer with oxygen.

The deposition reactor consisted of a glass cylinder 310 mm in diameter, 210 mm in height. The cylinder was enclosed by two discs of stainless steel. The lower electrode was capacitively coupled to a high frequency generator that is working at the usual frequency of 13.56 MHz. The films were deposited by plasma enhanced chemical vapour deposition in two steps, first the plasma pretreatment, which was a mean for improving the adhesion of the films to the substrate, and the second step was the deposition itself. The summary of the most important operational parameters are given in Table I.

3. Results and discussion

The surface energy of the plasma-treated polycarbonate immediately after the treatment, as well as ageing effects, was studied by contact angle measurements performing surface free energy measurements. The surface free energy of the deposited films was calculated according Lifshitz-Van der Waals/acid-base approach. This method enables us to determine the electron-acceptor and electron-donor parameters of the surface tension which is a sum of its apolar and polar components:

$$\gamma = \gamma^{LW} + \gamma^{AB} \text{ , with } \qquad \gamma^{AB} = 2\sqrt{\gamma^{+}\gamma^{-}} \qquad (1)$$

Here LW indicates the total apolar (dispersive) Lifshitz-Van der Walls interaction and AB refers to the acid-base or electron-acceptor/electron-donor interaction according to Lewis.

The surface free energy can be calculated according to Young-Dupré equation expressed by terms as acid component γ^+ (acceptor effect) and basic component γ^- (donor effect). The values can be determined from contact angle measurement with three liquids two of which must have polar component γ^{AB} (ref.[9]). If we use more than three liquids, the total surface free energy and its components may be determined by means of acid-base regression model[9].

The liquids we used and their table notations are as follows: water (w), glycerol (g), ethylene glycol (e), diiodomethane (d), formamide (f), and α-bromonaphtalene (b) on polycarbonate.

The results of plasma treatment optimization are illustrated in Fig. 1. We studied not only the immediate effect of the surface treatment on the polycarbonate surface free energy but also its stability during storage. In case of 10 minute nitrogen treatment at 50 W we obtained the highest surface free energy, however, its decrease with time was quite fast. Moreover, the long plasma treatment sometimes caused a slight change in the polycarbonate substrate color. We have found out, that the color change occurred in case of a long time storage of the polycarbonate. The polycarbonate tends to absorb water and therefore its water content increases with time. Under vacuum conditions there is a high water desorption. Using optical emission spectroscopy, we have found out that occurrence of water fragments in the plasma causes increase of optical emission intensity in the UV part of the spectra, which can cause photodegradation of the PC samples. Also, long time treatment increases the surface roughness. Therefore, the optimum treatment time was determined as 1 minute and the optimum gas was hydrogen. If applied power of 50 W was used, the initial surface free energy γ_{tot} was high enough to achieve good adhesion. The decrease of γ_{tot} was slow and during the short treatment time color change or increase in surface roughness was observed. What we observed was the fact that the coatings deposited on the pretreated samples had a better adhesion to the substrate. This is correlated with the decrease of the contact angle values and with the increase of the surface total free energy.

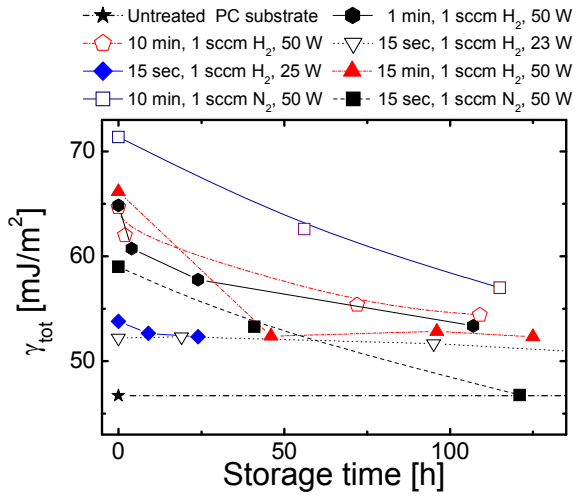

Fig. 1. **The dependence of the total surface free energy γ_{tot} on the storage time after plasma treatment in hydrogen or nitrogen.** The treatment time, gas flow and applied power are given in the graph

The values obtained from measurement of the contact angle for six liquids on thin films prepared from mixture of hexamethyldisiloxane and oxygen together with the values for the total surface free energy γ_{tot} and its components (γ^{LW}, γ^{AB}, γ^+, γ^-) are given in Table II. The results were obtained on films deposited on glass or polycarbonate substrate. The results listed in Table II. prove that the character of the thin film surfaces was possible to change from hydrophilic (for example VI15) to hydrophobic (for example VI12) .

In case of sample VI15, the polar component γ^{AB} as well as the acid γ^+ and base γ^- components were relatively high, compared to that of sample VI12. Sample VI12 had an almost purely apolar character, because the polar part of the surface free energy γ^{AB} was negligible.

Table II
Contact angle values Θ_i (suffix i denotes the liquid used: water – w, glycerol – g, ethylene glycol – e, diiodomethane – d, formamide – f, and α-bromonaphtalene – b) and total surface free energy γ_{tot} values together with their dispersive γ^{LW}, polar γ^{AB}, acid γ^{+} and base γ^{-} components for selected thin films. Film deposition conditions are given in Table I

Θ_w [°]	Θ_d [°]	Θ_g [°]	Θ_b [°]	Θ_e [°]	Θ_f [°]	γ_{tot} [mJ/m^2]	γ_{LW} [mJ/m^2]	γ_{AB} [mJ/m^2]	γ^+ [mJ/m^2]	γ^- [mJ/m^2]
VI15 on glass substrate										
43.56	55.71	41.46	31.16	33.55	–	45.96	34.19	11.78	0.96	36.07
VI13 on PC substrate										
83.79	58.48	79.97	34.67	58.64	57.65	34.91	34.13	0.78	0.03	5.81
VI12 on PC substrate										
86.74	62.01	81.02	49.67	67.29	69.65	29.6	29.11	0.49	0.01	6.35
VI08 on PC substrate										
49.82	47.52	41.85	30.59	–	–	47.15	34.46	12.69	1.5	26.77
VI01 on PC substrate										
80.6	62.47	76.39	49.98	66.27	60.43	30.97	28.95	2.02	0.11	9.23

The elemental composition, thickness and density, was determined by using the following nondestructive nuclear analytical methods[11], by RBS (Rutherford backscattering spectrometry) and ERDA (elastic recoil detection analysis).

The RBS is the only analytical method suitable for estimation of elemental composition in the whole depth of layers. The elements signals in RBS spectra overlap and this fact leads to great statistical uncertainty. We try to reduce this drawback by using enlarged non-Rutherford cross-section for proton projectiles scattered with C, O, Si. The conventional ERDA with 2.5 MeV alpha projectiles is suitable for hydrogen estimation up to depth 0.5–1 μm.

All spectra are at first evaluated severally and then each other interacted with regard for their definiteness. The right stopping powers depend on the precise composition of layers. For a detailed analysis of recorded experimental spectra, the codes GISA 3 (ref.[12]) and SIMNRA 6.06 (ref.[13]) were used.

Table III
Atomic composition of the prepared films obtained by RBS/ERDA

Sample	Si [%]	O [%]	C [%]	H [%]	O/Si ratio
VI06	21.46	59.41	0.13	19	2.77
VI07	29.86	51.15	0.48	18.5	1.71
VI08	30.23	52.52	0.75	16.5	1.74
VI10	27.27	58.51	0.72	13.5	2.15
VI15	27.12	54.72	1.66	16.5	2.02
VI16	27.11	54.7	1.9	18	2.02
VI19	20.43	32.85	20.72	26	1.61

The film deposited at relatively high negative self bias voltage and with HMDSO to total flow rate ratio around 0.5 or less exhibited SiO_2 – like properties. The carbon content in these coatings was low and the oxygen to silicon ratio was around 2 as it is in SiO_2 films (Table III) or more. In films prepared with n>0.5 and at relatively low negative self bias voltage the carbon and hydrogen content increased and these films showed polymer-like properties.

The instrumented indentation method and the Fischer scope H100 tester equipped with Vickers indenter was used to study the mechanical properties of the coating/substrate systems. The universal hardness HU can be defined as a measure of the material resistance against elastic and plastic deformation. From the loading/unloading curves it is possible to obtain the Martens hardness HM (measure of the resistance against elastic and plastic deformation). From the load-penetration curves (Fig. 2) it was possible to determine also the material resistance against plastic deformation H_{pl} (so called plastic hardness) or H_{IT} (so called indentation hardness) and the elastic modulus E_{IT} (Table IV).

The results in Table IV were obtained on films deposited on three different types of substrates (polycarbonate – pc, glass – gl, and silicon – si). The film thicknesses ranged from 3 to 5 μm. The substrate influence was negligible for silicon and glass substrates, but it is significant for polycarbonate, mainly in case of elastic modulus as it can be seen in Table IV. The results obtained on PC substrates characterise the resistance of film/substrate system against indentation at given indentation load. These parameters cannot be taken as the film characteristics. The results obtained on commercial paint used recently in the automotive industry for PC protection is included into graph and Table IV too.

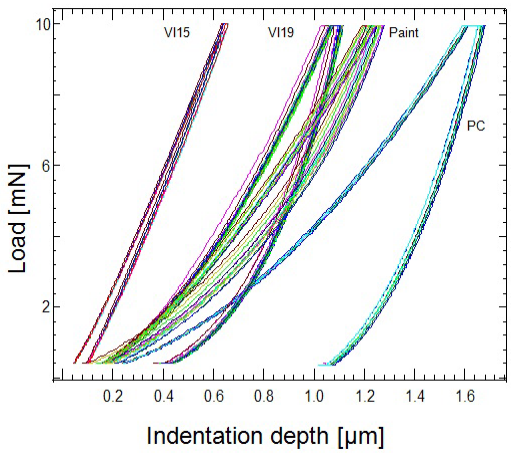

Fig. 2. **Comparison of the load-penetration curves obtained on noncoated PC and on PCs coated with films VI15, VI19 and commercial paint**

Jobin Yvon UVISEL phase-modulated spectroscopic ellipsometer was used to study the spectral dependences of prepared in films elipsin spectral range from 0.6 to 6.5 eV. Measurements were performed on five angles of incidence in the range 55° to 75°. The analysis of ellipsometric data of thick transparent films is generally difficult since it is not possible to use models assuming ideal layers and ideal apparatuses. Several effects, related to loss of coherence of light, become important for thick films even though they are not necessary to consider in the case of thin films. The final evaluation should take into account the effects of depolarization, which can be seen in spectral range from 0.6

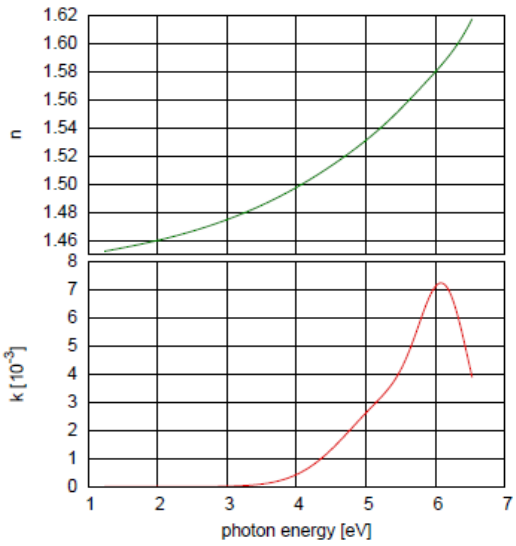

Fig. 3. **Spectral dependence of the refraction index n and the extinction coefficient k for sample VI19**

Table IV
Mechanical characteristics of the film-substrate systems on selected samples obtained using indentation tests with 10 mN of maximum load. HM is the Martens hardness, n_{IT} is the elastic to total deformation work ratio, H_{IT} is indentation hardness, E_{IT} is elastic modulus, h_{max} is the maximum indentation depth at maximum load of 10 mN, C_{r1} is the indentation creep deformation (expressed in percentage of h_{max}) reached during 5 s when the maximum load was kept constant, C_{r2} is the anelastic deformation (in percentage of h_{max}) reached during 5 s when the minimum load of 0.4 mN was kept constant. Abbreviation in sample name refer to the type of the substrate, i.e. pc – polycarbonate, gl – glass, si – silicon

No.	HM [GPa]	n_{IT} [%]	H_{IT} [GPa]	E_{IT} [GPa]	h_{max} [μm]	C_{r1} [%]	C_{r2} [%]
$VI06_{pc}$	0.16	55	0.32	3.1	1.56	2.4	–9
$VI07_{pc}$	0.17	52	0.33	3.5	1.49	2.7	–5
$VI08_{pc}$	0.14	52	0.25	3.0	1.68	2.2	–4
$VI10_{pc}$	0.15	59	0.29	3.3	1.57	2.3	–6
$VI15_{pc}$	0.70	92	11.8	18	0.74	0.9	–4
$VI16_{pc}$	0.69	91	10.8	18	0.74	0.9	–4
$VI19_{pc}$	0.21	88	0.82	3.7	1.35	1.4	–7
$VI06_{gl}$	3.33	65	8.54	68	0.35	1.2	–2
$VI07_{gl}$	3.67	60	8.27	79	0.32	1.5	–1
$VI08_{gl}$	3.03	60	6.93	63	0.35	1.6	–
$VI10_{gl}$	3.83	74	11.8	69	0.33	0.1	–
$VI16_{gl}$	3.43	70	9.80	69	0.33	0.9	–
$VI15_{si}$	3.48	68	9.50	70	0.33	0.7	–
$VI19_{si}$	0.59	93	2.24	11	0.80	0.5	–
Paint	0.27	64	0.56	5.4	1.18	2.9	–8
Substrates							
PC	0.12	41	0.19	3.1	1.74	2.9	–3
Glass	3.77	58	9.25	81	0.31	0.4	–
Si	7.32	62	13.3	18	0.28	–	–

to 1.25 eV and was caused by reflection of light from back side of the transparent silicon wafer.

In Fig. 3 an example of the dependence of the refractive index *n* and the extinction coefficient *k* on the photon energy obtained for film VI19 is shown. There is a strong increase in extinction coefficient in the spectral region from 4 to 6 eV, so the absorption of film VI19 increased in UV region. The thickness of the film VI19 was determined from ellipsometric measurements as t = 5320±20 nm.

4. Conclusion

Multifunctional thin films were prepared in r.f. capacitively coupled glow discharges using controlled ratios of mixtures between hexamethyldisiloxane with oxygen and hexamethyldisilazane with nitrogen on the polycarbonate substrates. By varying the discharge parameters

and the gas flow rates it was possible to change the character of films from hydrophobic (γ_{tot} =28 mJ m^{-2}) to hydrophilic (γ_{tot} = 47 mJ m^{-2}), from soft polymer-like (H_{IT} = 1 GPa, E_{IT} = 10 GPa) to hard SiO_x-like (H_{IT} = 11 GPa, E_{IT} = 80 GPa) films. The films were fully transparent for the visible light, the absorption in UV region for photon energy higher than 4.5 eV was observed for polymer-like films.

This research was supported by the Grant Agency of the Academy of Sciences of the Czech Republic under contract KAN311610701, by the project CZ.1.05/2.1.00/03.0086 'R&D center for low-cost plasma and nanotechnology surface modifications' funded by European Regional Development Fund and by the Ministry of Industry and Trade, contract FTTA5114 and by the Ministry of Education, Youth and Sports of the Czech Republic, contract MSM 0021622411

REFERENCES

1. Borcia C., Borcia G., Dumitrascu N.: Appl. Phys., A *90*, 507 (2008).
2. Sepeur S., Kunze N., Werner B., Schmidt H.: Thin Solid Films *351*, 216 (1999).
3. Zajickova L., Bursikova V., Janca J.: Vacuum *50*, 19 (1998).
4. Rats D., Hajek V., Martinu L.: Thin Solid Films *340*, 33 (1999).
5. Rivaton A.: Polym. Degr. Stab. *49*, 163 (1995).
6. Ram A., Zilber O., Kenig S.: Polym. Eng. Sci. *25*, 535 (1985).
7. Tjandraatmadja G. F., Burn L. S., Jollands M. C.: Polym. Degr. Stab. *78*, 435 (2002).
8. Benz G., Mutshler G., Schneider G.: Germany Patent DE 3413019 (1985).
9. http://www.makrolon.de. (7.9.2012)
10. Buršíková V., Sťahel P., Navrátil Z., Buršík J., Janča J.: *Surface Energy Evaluation of Plasma Treated Materials by Contact Angle Measurement*. Masaryk University, Brno 2004.
11. Wang Y., Nastasi M.: *Handbook of Modern Ion Beam Materials Analysis*, Second Edition. Materials Research Society, Warendale, Pensylvania 2009.
12. Saarilahti J., Rauhala E.: Nucl. Instrum. Methods Phys. Res. *B64*, 734 (1992).
13. Mayer M.: *SIMNRA User`suide, Technical report IPP 9/113*. Max-Planck-Institut fur Plasmaphysick, Garching, Germany 1997.

V. Mocanu[a], A. Stoica[a,b], L. Kelar[a], D. Franta[a,b], V. Buršíková[a,b], R. Mikšová[c], and V. Peřina[c] *([a] Dept. of Physical Electronics, Masaryk University, Brno, [b] CEITEC, Central European Instituteof Technology, Masaryk University, Brno, [c] Nuclear Physics Institute, Academy of Sciences of the Czech Republic, Rež near Prague, Czech Republic):* **Multifunctional Transparent Protective Coatings on Polycarbonates Prepared Using PECVD**

Thin transparent films on polycarbonate substrates were prepared using a capacitively-coupled radio-frequency discharge. The films were obtained from mixtures of hexamethyldisiloxane with oxygen. Varying the discharge parameters and the gas flow rates, multifunctional coatings wre prepared. The films were analysed using depth sensing indentation method, contact angle measurements, surface energy calculation, ellipsometry and spectrophotometry in order to determine the properties and functionality (hardness, fracture toughness, adhesion, internal stress, abrasion resistance, thickness, color, refractive index) of the obtained structures. The behavior of the coatings covers a wide range of material properties from inorganic to polymer-like coatings.